SEMMELWEIS EGYETEM

DOKTORI ISKOLA

# Ph.D. értekezések

## 3458.


## ELEK RICHÁRD


**Celluláris és molekuláris biofizika**
című program

Programvezető: Dr. Kellermayer Miklós, egyetemi tanár

Témavezető: Dr. Osváth Szabolcs, egyetemi adjunktus

# RADIATION RISK AND IMAGE QUALITY ASSESSMENT OF DIGITAL VARIANCE ANGIOGRAPHY
## In-vivo multimodal preclinical imaging

**Ph.D. thesis**


**Richárd Elek**

Semmelweis University Doctoral School

Theoretical and Translational Medicine Division




Supervisor: Szabolcs Osváth, Ph.D.

Official reviewers: Szabolcs Czifrus, Ph.D.
Károly Liliom, Ph.D.

Head of the Complex Examination Committee:
György Reusz, MD, Ph.D., D.Sc.

Members of the Complex Examination Committee:
Orsolya Kiss, Ph.D.
Ákos Jobbágy, Ph.D.

Budapest

2026

# Table of contents

**List of abbreviations** ..... **3**

**1. Introduction** ..... **4**

**2. Objectives** ..... **9**

**3. Methods** ..... **10**

3.1. Validation of dosimetric quantities ..... 10

3.2. Risk assessment of angiographic procedures ..... 11

3.2.1 Data collection for PAD procedures ..... 13

3.2.2 Data collection for PAE procedures ..... 14

3.2.3 Qualification of the source ..... 14

3.2.4 Quantification of the source ..... 14

3.2.5 Settings for the simulations ..... 15

3.2.6 Organ dose and cancer risk estimation ..... 19

3.3. Comparative assessment of DVA and DSA ..... 22

3.3.1 PAD procedures' evaluation ..... 22

3.3.2 PAE procedures' evaluation ..... 23

3.4. Objective image quality assessment ..... 24

**4. Results** ..... **27**

4.1. Validation of dosimetric quantities ..... 27

4.2. Risk assessment of angiographic procedures ..... 27

4.2.1 PAD procedures' risk assessment ..... 27

4.2.2 PAE procedures' risk assessment ..... 28

4.3. Comparative assessment of DVA and DSA ..... 29

4.3.1 PAD procedures' evaluation ..... 29

4.3.2 PAE procedures' evaluation ..... 30

4.4. Objective image quality assessment ..... 34

**5. Discussion ..... 35**

5.1. Validation of dosimetric quantities ..... 35

5.2. Risk assessment of angiographic procedures ..... 35

5.2.1 PAD procedures' risk assessment ..... 38

5.2.2 PAE procedures' risk assessment ..... 38

5.3. Comparative assessment of DVA and DSA ..... 38

5.4. Objective image quality assessment ..... 39

**6. Conclusions ..... 40**

**7. Summary ..... 42**

**8. References ..... 44**

**9. Bibliography of the candidate's publications ..... 58**

9.1. Publications related to the present work ..... 58

9.2. Unrelated publications ..... 58

**10. Acknowledgements ..... 60**

**List of abbreviations**

| | |
|---|---|
| AERC | Automatic Exposure Rate Control |
| BEIR | Biological Effects of Ionizing Radiation |
| CED | Collective Effective Dose (CED, see ED) |
| DICOM | Digital Imaging and Communications in Medicine |
| DSA | Digital Subtraction Angiography |
| DVA | Digital Variance Angiography |
| ED | Effective Dose (originally $E$, changed for clarity) |
| ESAK | Entrance Surface Air Kerma |
| FLU | Fluoroscopy |
| IAK | Incident Air Kerma |
| ICRP | International Commission on Radiological Protection |
| IQTO | Image Quality Test Object |
| IR | Interventional Radiology |
| KAP | Kerma-Area Product (≈ dose-area product, $P_{\mathrm{KA}}$) |
| KMIT | Kinepict Medical Imaging Tool |
| kVp | Kilovolt peak (of the set X-ray tube voltage) |
| LAR | Lifetime Attributable Risk |
| MC | Monte Carlo (simulations) |
| MPV | Mean Pixel Value |
| ND | Normal Dose |
| PAD | Peripheral Arterial Disease |
| PAE | Prostatic Artery Embolisation |
| PENELOPE | PENetration and Energy LOss of Positrons and Electrons |
| RDSR | Radiation Dose Structured Report |
| ROI | Region of Interest |
| rpm | Revolutions per Minute |
| SA | Stationary Acquisition |
| SD | Standard Deviation (of pixel values) |
| ULD | Ultra-low Dose |
| UNSCEAR | United Nations Scientific Committee on the Effects of Atomic Radiation |

## 1. Introduction

Without any hesitation everyone accepts the fact that the discovery of X-rays and its use in medicine brought tremendous aid to advance the welfare of mankind. While ionising radiation has its benefits, the early years after its discovery has demonstrated that it is not without risks [1], leaving a lasting memory and calling for action [2–6]. To this end, a framework for radiation protection was necessary [7]. According to the current concept of protection [8], exposures incurred by patients – whether symptomatic or asymptomatic – that are undertaken for any reason with a real or potential health benefit must be both justified and optimised. Justification is an issue to be judged strictly by the relevant medical professionals, referrers and practitioners [9,10]. Most often guidelines are available for these [11], taking years for professional societies to ponder the results of research efforts from evidence-based medicine to select the best practices. Optimisation is a continuous effort to achieve the lowest prospective radiation detriment from the radiological procedure while achieving the sufficient outcome of the given procedure. One must note however, that in the context of medical exposures, one of the main principles of radiation protection, namely 'Limitation', cannot be applied as this would jeopardise the clinical outcome [8].

Interventional radiology (IR) is a minimally invasive technique to facilitate the introduction of devices into the body using image guidance. It may be used to diagnose and treat several lesions, but from the medical physicists' perspective it is a diagnostic procedure which may utilise the physical properties of ionising radiation, namely that different components of the human body have differing attenuation properties and X-rays can be used to exploit this phenomenon. IR using X-ray imaging techniques (referring to IR as such from hereon) is considered as a source of medical exposures and has risen in terms of frequency by more than five-fold in the past decade [12,13], due to its increased accessibility and longer expected life span. Circulatory diseases occupy the pole positions among the leading causes of death in developed countries [14–16]. These may be either diagnosed or treated by IR, depending on the individual patient, but paradoxically ionising radiation, a carcinogenic agent may lead to the second most prevalent cause of death, cancer. As the most recent report of the United Nations Scientific Committee on the Effects of Atomic Radiation (UNSCEAR) highlights it [13], IR deserves further scrutiny, as it contributes only 0.6% to the number of medical procedures, but contributes

8.0% to the collective effective dose (CED) when one consider the average annual medical exposure of patients' effective doses (ED). This substantial contribution is explained by the fact that radiation doses from IR procedures may exceed those associated with most other medical diagnostic procedures [17–21] and are considered "high dose" procedures.

To optimise IR procedures, one may employ several tools [22–25]. In any case it requires a close cooperation of the practitioner, the medical physicist and other staff members [10,26] to achieve its aim. The tools for optimisation include those which are inherently available for every IR system, such as the adjustment of the X-ray beam quality (by adding filtration and/or lowering the applied tube voltage), lowering the X-ray fluence (reducing the mA and/or irradiation time), and more strict confinement of the beam. Furthermore, optimisation could rely on the routine of the practitioner and the available imaging techniques (e.g., roadmap, last image hold, etc.) [27]. However, another opportunity is to use new imaging technologies and novel image processing algorithms which may help with the visualisation of vessels. A prime example of such a novel imaging technique is Digital Variance Angiography (DVA) also dubbed kinetic imaging. This image processing technique has the same goal as Digital Subtraction Angiography (DSA). DSA is the prevalent image processing method [28] to visualise contrast media in vessels (Fig. 1). Both image processing methods aim to enhance contrast media visualisation in the vessels in order to enable the unobstructed view of blood flow by removing the radiopaque background structures from the images.

DVA was invented by two fellow researchers of our University, Szabolcs Osváth Ph.D. and Krisztián Szigeti Ph.D., who founded a startup, Kinepict Health Ltd., in 2015 and patented the DVA imaging technology [29,30]. Although several studies have demonstrated the efficacy of DVA [31–43], these are limited to the exploration of dose reduction in terms of physical dosimetric quantities, the reduction of iodinated contrast media or the use of carbon-dioxide and quantification of the improved diagnostic insight which DVA provides. This thesis had the aim to assess the impact of the technology in terms of ED and other associated radiological risk metrics.

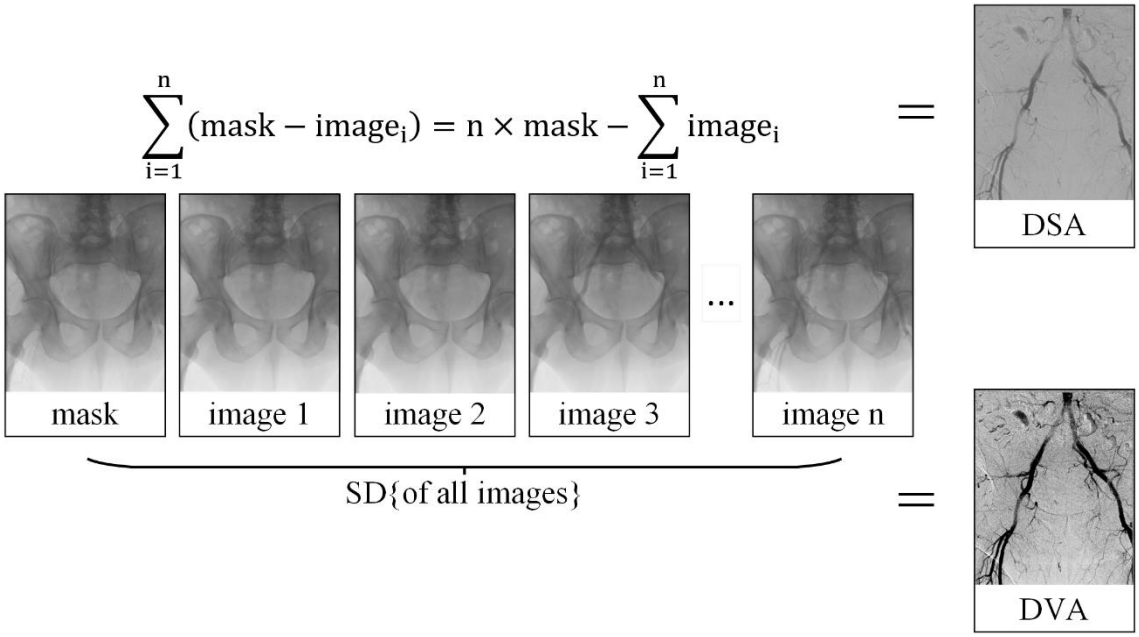


*Fig. 1. In Digital Subtraction Angiography (DSA, top), the first image of the series is typically used as a mask, and it is subtracted from all subsequent images to highlight contrast-enhanced structures. These could be then summed as here or merged in another way. On the contrary, Digital Variance Angiography (DVA, bottom) processes the entire image series to enhance the visibility of vascular structures by leveraging temporal statistical properties (i.e., the standard deviation or SD). This figure illustrates the image processing principles of DSA and DVA and shows their respective outputs.*

Since ionising radiation is a carcinogenic agent, but its level is considered to be closely correlated with the expectable health detriment, this level is the de facto indicator of its cancer inducing effect. Radiological risk assessment in turn can rely on several metrics to estimate risks from this radiation level, such as the commonly adopted ED and the less ubiquitous lifetime attributable risk (LAR) of cancer incidence and mortality, which also has its own proponents for medical exposures [8,44–46]. Other descriptors which could be used for the evaluation of the benefits brought by utilising DVA could involve the estimation of quality adjusted life years, commonly found in health economics evaluation studies. This metric is criticised for its methodological and ethical approach as it tries to associate utility of care with health [47]. Contrary to the effort to introduce any new ways of evaluation, even involving complex numbers, the underlying problems remained [48]. Further metrics were proposed in the literature, such as life years, equal

value life years and health years in total, each having their own shortcomings [49]. These are rejected in this thesis and only radiological risk assessment is considered to establish a relation between physical dosimetric quantities and stochastic risks arising from the exposure due to ionising radiation.

Any radiological risk descriptor used shall rely on information about the imaging system in question and have an adequate indicator of a physical dose metric, such as incident air kerma (IAK), entrance surface air kerma (ESAK), reference dose at the interventional reference point, radiation output or air kerma-area product (KAP) [50]. The given physical dosimetric quantity will then enable the use of conversion coefficients to translate the preceding physical radiation level to radiological risks. The determination of conversion coefficients seldom rely on other than the Monte Carlo (MC) method, but finite element methods and experimental assessments can also be used for this, albeit more expensive and having significant flaws [51]. MC methods do not have an exact definition, but have been used since the Manhattan project to solve radiation transport problems. The method involves random sampling of the probability distributions of the particle's behaviour, i.e., cross-section data to determine individual particle interactions in complex geometries, such as the human body. The method is computationally intensive because individual particles yield insignificant results. To put it more simply, it is a gamble where following the destiny of millions or billions of particles through a complex geometry on a particle-by-particle basis will reveal the outcomes of interest which may be impossible to measure or determine otherwise [52]. For the modelling of medical exposures, deposited energy, particle distribution or spectra may be of utility. For studying radiological risks, it is the deposited energy in an organ which is then used to estimate the organs' absorbed doses. The use of MC methods for this purpose started in the sixties and the advent of computing capacity broke the barriers to become a hallmark of medical physics nowadays as we know [53,54]. Due its aforementioned characteristics and robustness, this "gold standard" method is used in my work.

Another key question for this thesis is the objective evaluation of image quality, vindicating that X-ray images are acquired at the cost of radiation dose. There are several image metrics which could be used to characterise the contrast enhancement properties of angiographic image processing techniques, such as noise, signal-to-noise ratio, contrast, contrast-to-noise ratio (CNR), high-contrast spatial resolution and others. From

these, the most commonly used and most robust one is CNR, but this cannot be deemed as a singular and definite descriptor of image quality. The use of CNR and dose to specify a figure of merit would have limitations, but can have special applications [55]. The objective angiographic image quality assessment has been sought by researchers for a long while and several quite interesting proposals were published with both static and dynamic phantoms. The former is obviously inadequate for the evaluation of constant changes in the attenuating properties of contrast media filled vessels, the vascular densities. The latter may require consumables, may be cumbersome to use or lack portability [56]. There are standardised image quality test objects (IQTO) for the image quality assessment of DSA with a handpump and an insert which have two possible positions [57–59]. These are also unsuitable to assess the image quality of DVA as all of these DSA contrast detail phantoms have binary positions of their inserts which simulate the flow of contrast media (Fig. 2).

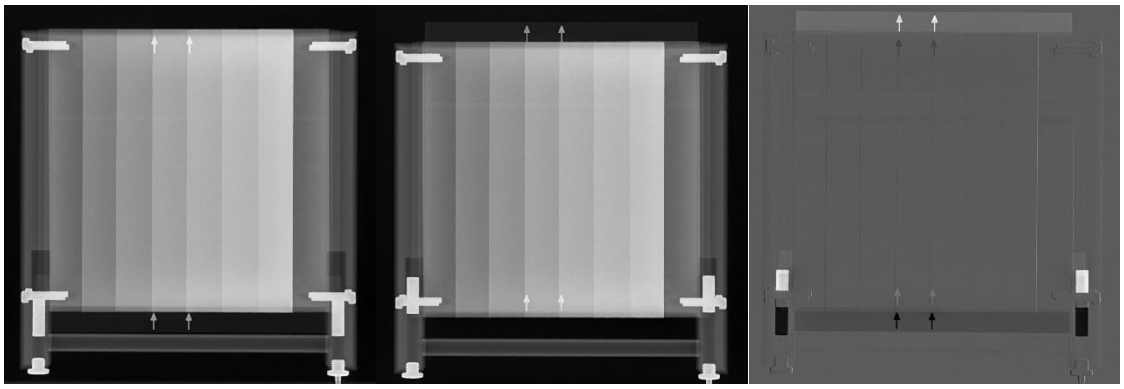

*Fig. 2. X-ray image of a dynamic test object used for digital subtraction angiography (DSA). Visual cues (arrows) at the bottom and top indicate the insert's position.*

Addressing these issues was essential to support the clinical commissioning of the Kinepict Medical Imaging Tool (KMIT), the computational framework for DVA, in IR suites and to quantitatively demonstrate its benefits using an IQTO. A further motivation for the development of an IQTO is that commissioning tests and training of medical staff may be conducted in a safe and reproducible manner.

Overall, this thesis presents a comprehensive evaluation of DVA technology, integrating both radiation dose and risk assessment with objective image quality analysis, thereby providing a quantitative demonstration of DVA's clinical benefits.

## 2. Objectives

My working hypothesis, based on earlier findings on physical dose reduction, was that DVA could be more efficient than DSA in reducing radiological risks while providing better image quality. The aim is to provide quantitative evidence on the effects of DVA in terms of ED reduction, LAR and image quality compared to DSA. In order to estimate radiation risks, one must first determine the organ absorbed doses from each image series of the angiographic procedure [45]. This is done by calculating the amount of energy deposited in organs during the procedures, most usually by the means of MC simulations. Then the results of this calculation could be used to estimate ED, LAR of cancer incidence and mortality and analyse the data to provide the necessary evidence for prospected patient dose reduction. There are no off-the-shelf solutions to solve this problem, thus it was also necessary to develop the data mining tools and computer codes because of the large number of irradiation events that had to be analysed.

Image quality is inseparable from dose and therefore risk [60]. For the set goals, a new kind of IQTO had to be developed which would be able to help objectively discern the motion and change of contrast media in vessels.

Brief summary of goals:

1) Further validation of dosimetric quantities to provide a solid basis for our studies.
2) Development of a particle transport simulation framework based on a generic, validated MC simulation software suite.
3) Estimate risks from clinical studies and analyse data to provide evidence for the efficacy of DVA.
4) Develop a test device (IQTO) and establish a methodology for the objective evaluation of DVA image quality enhancement.

## 3. Methods

The methods section is based on the publications related to the present work [61] and [62]. Both publications are published under the CC BY 4.0 terms: https://creativecommons.org/licenses/by/4.0/

Both clinical studies referenced in this work have undergone ethical approval.

The clinical study of Sótonyi et al. on Peripheral Artery Disease (PAD) procedures [63] provided data for the presented risk assessment study [61]. This study was approved by the Hungarian National Institute of Pharmacy and Nutrition (reference number OGYÉI/2830/2017). All study activities were in accordance with the ethical standards of the Hungarian Medical Research Council and with the 1964 Helsinki Declaration. The study protocol is available on clinicaltrials.gov (NCT04343196). Written informed consent was obtained from all participants included in the study.

The Institutional Review Board of the Frankfurt University Hospital approved the study [62] (ref. 2022-941), and all patients provided written informed consent.

### 3.1. Validation of dosimetric quantities

Since the work involved estimating organ absorbed doses, the first step was to review the accuracy of the physical dosimetric quantities displayed by the X-ray angiographic units used in the investigations.

One such X-ray angiography unit was a Siemens Artis Zee Floor machine at the Heart and Vascular Centre of Semmelweis University. This was used for the study by Sótonyi et al. on PAD procedures [63]. Another machine was a General Electric Innova IGS 540 unit at the Semmelweis University Medical Imaging Centre. I used a PTW UNIDOS Webline electrometer and a legally verified 30013 Farmer-type ionisation chamber (PTW Freiburg GmbH., Freiburg, Germany) set in the lowest range for integrated charge measurement to calibrate dose indices. I have also used an RTI Piranha 657 X-ray multi-meter to measure the half-value layer and total filtration of the X-ray machines. The X-ray units are under a quality assurance programme [64,65].

I employed a methodology, which follows internationally accepted standards [50] to determine IAK and ESAK (see Fig. 3) and to validate the displayed KAP which is based on IAK. Since the cumulative current-time product for the different automatic

exposure rate control (AERC) settings may be relatively small, at least 40 frames were used for each setting.

The prostatic artery embolisation (PAE) study was conducted on a recently commissioned, state-of-the-art Siemens Artis pheno interventional machine at the Frankfurt University Hospital. This device is also under a quality assurance program and dosimetric indicators were verified at the time of acceptance test [64].

*Fig. 3. Geometrical set-up for the measurement of ESAK (left, includes backscatter) and IAK (right, without backscatter) which were used to determine the accuracy of displayed dose indices.*

### 3.2. Risk assessment of angiographic procedures

DVA enhances stationary acquisitions (SA) only as it is not designed to enhance fluoroscopic (FLU) image sets or rotational and other imaging series. Only SA were used for the comparison between DSA and DVA; therefore, dose and irradiation geometry data corresponding to these acquisitions were extracted from the angiographic units' workstation. No other imaging modalities were used for the angiographic procedures. As mentioned previously, this task requires the development of a framework to automate the

process of extracting data from the Digital Imaging and Communications in Medicine (DICOM, or DCM) files exported from the angiographic units for which, there are no off-the-shelf solutions [66–69]. Data processing then requires parsing of the necessary information for the input of the particle transport simulations. The next figure (Fig. 4) illustrates the workflow of data processing, while the subsequent sections explain software choices made throughout the project.

Python (v3.9) was selected as the implementation language for the framework. The accuracy of the extracted data was double-checked manually, by comparing the information read-out from the DICOM headers with those displayed by DICOM viewer applications (OFFIS DCMTK, ImageJ, MicroDICOM) to validate the accuracy of the script for data extraction.

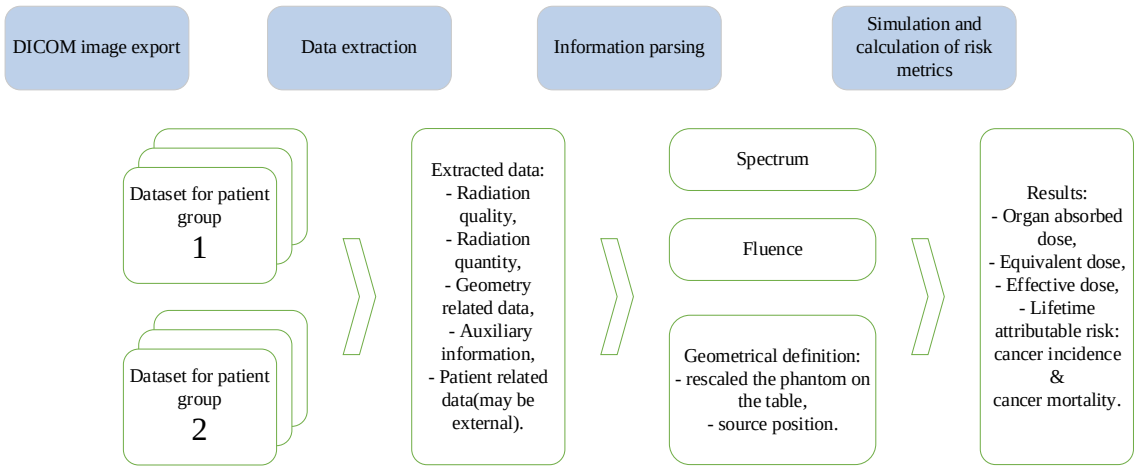


*Fig. 4. The workflow of the particle transport framework. Group 1 and group 2 denotes the DVA and DSA groups for the study on PAD procedures and it denotes the normal dose (ND) and ultra-low dose (ULD) groups for the PAE procedures' study. First, a DICOM image series data export is necessary using the metadata of the headers. Then the algorithm extracts the data for each irradiation event and their corresponding exposure parameters. Patient related data are supplied externally (age, height, weight). Based on the parsed data, particle fluence and energy distribution are determined along with the definition for the geometry of the irradiation event. After running the simulations, risk related metrics (ED and LAR) are calculated based on the organ absorbed doses determined by the MC simulations.*

The following table (Table 1) summarises the DICOM tags and their corresponding identifiers used in the framework.

*Table 1. DICOM data tags extracted from image series. Adapted from [61].*

| | |
|---|---|
| Identification | Image unique identifier (UID) (0008,0018); patient name (0010,0010, anonymised as 'patient_X') |
| Patient-related data | Patient age (0010,1010), patient sex (0010,0040); |
| Radiation quality | X-ray tube voltage peak value, kVp (0018,0060); added filtration (0021,100a); |
| Radiation quantity | KAP (0018,115e); |
| Irradiation geometry-related information | Patient position (0018,5100);<br>Source to image receptor distance (0018,1110);<br>Primary angle (0018,1510); Secondary angle (0018,1511);<br>Table position (0021,1057) as Lat.\Long.\Height coordinates*;<br>Shutter and collimator related data (0018, 1600; 1602; 1604; 1606; 1608 and 0018,1700; 1702; 1704; 1706; 1708), including pixel spacing (0018, 1164) to calculate the field size. |
| Auxiliary information | Patient height and weight. These were available separately as no DICOM tags encoded this information. |

* Checked experimentally

### 3.2.1 Data collection for PAD procedures

Building on the randomized controlled trial study by Sótonyi et al. [63] on PAD procedures, the exposure data from all patients for a comprehensive analysis was extracted using the methods detailed in this section. The exposure data from each image series was closely reviewed, including those from the Radiation Dose Structured Report files (RDSR), and study summaries. If any of the exposure data, image count, or series count did not exactly match, the entire dataset of the procedure for that patient was excluded. Ultimately, 107 out of the 114 patients met the above inclusion criteria. Among these, 54 patients underwent angiographic procedures using DVA, while 53 underwent the procedure with traditional DSA for an assessment of their condition.

### 3.2.2 Data collection for PAE procedures

The normal dose (ND) group (35 patients), pre-installed DSA acquisition protocols (CARE aorta and CARE pelvis; 1.17 μGy/frame, 4 fps) were used in this randomized controlled trial. In the ultra-low dose (ULD) group (35 patients), radiation dose was reduced by decreasing the target detector dose level of the same protocols to 28%, while imaging parameters were adjusted by the angiography unit. Procedural aspects were unchanged. Dose indices and the protocol-related data (Table 1) were obtained from the RDSR files. Both the ND and ULD patient groups' image sets were processed with DSA and DVA.

### 3.2.3 Qualification of the source

PENELOPE version 2018 (PENenetration and Energy LOss of Positrons and Electrons, via the Nuclear Energy Agency Data Bank) was used to simulate particle transport inside the patient by the X-ray irradiation. In order to initiate simulations in PENELOPE, one has to provide the source term, which in this case was a point-like X-ray source with the parameters determining radiation quality, kVp and the added filtration of the actual image acquisition. Total filtration was determined to be at least 2.8 mm Al equivalent without additional filtration, see Section 3.1. Depending on the imaging protocol, machine selectable additional filtration can be 0.1 to 0.9 mm Cu. SpekPy [70–72] was used to generate the corresponding X-ray spectra based on the selected kVp and filtration settings, using a bin width of 1 keV as this approach may be considered the most novel one, due to its analytical method [72–80]. The X-ray source was considered to be a simple point source, while the inhomogeneity of the X-ray field due to the heel-effect, extra-focal radiation and the penumbra and the voltage ripple effects are neglected.

### 3.2.4 Quantification of the source

Another key aspect of the source term is the number of quanta emitted during an irradiation event. The number of quanta (i.e. the total number of photons emitted from the X-ray tube during an exposure), *N*, was calculated using the following formula (eq. (1)):

$$N = \frac{KAP \times \rho_{air}}{\sum_n p_n E_n \mu_{en,n}} \quad (1)$$

where $\rho_{air}$ is the density of air (g/cm$^3$) under standard conditions at sea level. Since the number of photons emitted by the source depends on the X-ray spectrum, the spectrum calculated in the previous step of the workflow was used to determine *N* by summing over the *n* energy bins, to account for the contribution of each bin to the total energy fluence (J). The terms in the denominator describe this contribution ($p_n E_n$) multiplied by the linear energy absorption coefficient, $\mu_{en,n}$ (1/cm). The verification of KAP (mGy×cm$^2$) is described in Section 3.1.

### 3.2.5 Settings for the simulations

The following figure (Fig. 5) illustrates the geometrical arrangement modelled for the simulated irradiations. The isocentre is a hypothetical point in space through which the X-ray beam passes through from the source to the image receptor and determines the central axis of the projection. Knowing the position of this point serves as a reference to calculate the source position based on the angulation of the C-arm.

Angiographic X-ray systems describe the relative position of the beam using an isocentre-based coordinate system, where the patient position, the source-to-image distance, the angles and the table positions shall be known to orient the irradiated part of the body, as referenced in Table 1. The next figure (Fig. 5) illustrates how each of these parameters is incorporated into the simulation geometry.

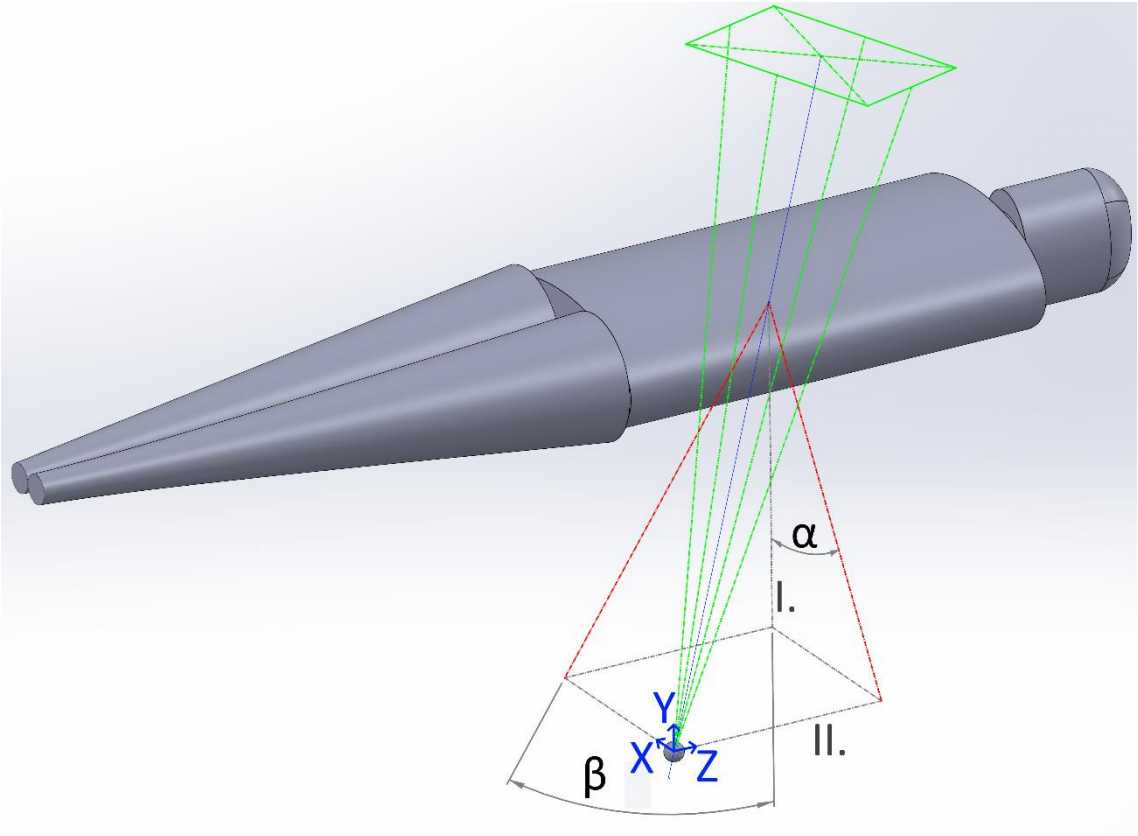


*Fig. 5. Illustration of the anthropomorphic phantom lying on its back. The grey sphere at the bottom of the image represents the X-ray source. The thin blue line connecting the centre of the image plane with the source indicates the main axis of the beam. The isocentre is the centre of rotation, incident on the X-ray beam's main axis. The isocentre's projection is a vertical grey line (I.) perpendicular to the laboratory reference frame's X-Z plane (II.). Position of the C-arm is determined by the primary and secondary angles measured from the isocentre's vertical projection. The lowercase Greek letters α and β denote the primary and secondary angles, respectively. The green lines at the image plane illustrate the rectangular radiation field. The operating table and the mattress below the patient were taken into account in the simulations, but are not shown in this figure for the sake of discernibility.*

Using the available descriptors of the geometric setup the exact position of the source can be determined through basic trigonometric calculations. However, significant uncertainty in estimating each patient's radiation exposure may arise from the positioning approach – such as head-centred or alternative reference points – is used during modelling. In the referenced clinical studies [62,63], the clinical personnel maintained a

fixed distance of 5 cm from the head end of the table and used this consistent positioning of the patient. This is duly accounted for in the positioning of the patient for the geometrical model. The X-ray beam is confined to the target body region by the shutter and collimator. However, beam size information is provided in terms of number of pixels at the image plane rather than in metric units. Therefore, pixel spacing must be taken into account to determine the exact field size at the image plane. The calculation of this is essential, as this leads to another simple trigonometric calculation to estimate the apex angle for the SRECTA parameter in the simulation, i.e., the beam's extent around the main axis.

Quadric geometry adult mathematical phantoms were used which are included in the PENELOPE 2018 simulation package [81]. Models of male and female patients are based on the adult-type phantom, excluding organs that are not present for the corresponding sex (breast, uterus and ovaries for males; prostate and testes for females). Since these models do not include several organs, earlier works were used to enhance the model [82,83] and be able to estimate organ doses with significance according to ICRP 103 [8]. Table 2. gives an overview of the organs defined in the model. Using quadric geometries to define bodies building up the patients' organs opens up the possibility to rescale the computational phantom easily and match the actual patient's habitus. The "PCXMC" user manual [84] describes a simple method to apply scaling factors to better match the mathematical phantom to the patients' actual physical size.

The following scaling factor (eq. (2)) was used to match the patient's height, $h$, in direction Z:

$$s_z = \frac{h}{h_0} \tag{2}$$

is used to establish a simple relation, where $s_z$ is the scaling factor and $h_0$ is the phantom's height (178.5 cm).

To account for the patient's weight $M$, the ellipsoid cross-section of the phantom in the X-Y direction can be changed using the following scaling factor, $s_{xy}$ (eq. (3)):

$$s_{xy} = \sqrt{\frac{h_0\, M}{h\, M_0}} \tag{3}$$

where $M_0$ is the phantom's unscaled weight.

Using these scaling factors, the coordinates of each point in the phantom are transformed as follows (eq. (4)):

$$x = s_{xy}x_o \qquad y = s_{xy}y_o \qquad z = s_z z_o \tag{4}$$

This modelling approach was adopted despite its known limitation: it does not account for variations in body composition such as fat distribution. Nevertheless, the method assumes that the scaling affects the positions, sizes, volumes, and masses of the organs, which are adjusted accordingly.

Various methods are described [67,85,86] how to account for the scattering and attenuation properties of the patient support and the mattress or pad under the patient. The table's physical dimensions were measured, and it was modelled as a homogenous body made of carbon fibre and epoxy resin (elemental ratio: 0.713% H, 96.022% C, 2.262% O, 1.003% Cl), having a density of 1.79 g/cm$^3$.

Each irradiation event was run individually as a single process. Several simulations were run on the same computer simultaneously. Each irradiation's simulation was initiated with 1 million showers to provide reliable statistics but a relatively low computing time of ≈ 15 minutes. Although these simulations were relatively quick, they still allowed the statistical uncertainty of each simulation to stay below 5% for all organs in the beam. Electron and photon cut-off energies were chosen to be the default (1/100th of the maximum) and no variance reduction techniques were used.

PENELOPE is a general purpose, coupled photon-electron transport MC simulation code, thus it does not simplify or neglect any significant interactions. This is important, because the interactions at the X-ray energy levels relevant to the study are fully accounted for in the calculation of the mean energy absorbed by each organ. Consequently, the organs partly aligned with the X-ray field absorb the appropriate fraction of the primary photons' energy but with higher statistical uncertainty than the previously cited 5%, depending on their overlap with the field. Those organs' mean absorbed dose which are not in the radiation field are much smaller, but have a higher uncertainty.

### 3.2.6 Organ dose and cancer risk estimation

To have a critical evaluation of stochastic risks which may arise from the radiological procedures (DVA and DSA), the absorbed dose of each organ was calculated and weighted by the tissue weighting factors recommended by the ICRP [8]. The absorbed dose of an organ ($D_{organ}$) is calculated with the following equation (eq. (5)).

$$D_{organ} = Nk\frac{\sum \bar{E}_{body,organ}}{M_{organ}} \tag{5}$$

where $\bar{E}_{body,organ}$ is the mean energy absorbed in each body in eV units. The total mass of the organ is $M_{organ}$ in kg. $N$ is the number of photons obtained from equation (1). The conversion coefficient, $k$, is $1.602176565\times10^{-19}$ J/eV.

The above approach was applied to all organs except the active (red) bone marrow and the lymphatic nodes. For these, a different estimation method was used due to modelling challenges and the need for computational efficiency. The distribution of the active bone marrow in different bones of the present model can be found in the original report [87–89] published by Oak Ridge National Laboratory. Bones also contain inactive (yellow) bone marrow but only red bone marrow is considered to be radiation sensitive. Red bone marrow has lower electron density than bone, but bones are present in the model as homogenous bodies. The spectral distribution of the absorbed energy in the bone should be known to account for the underestimation of dose to the red bone marrow. This underestimation could be corrected by applying the ratio of the mass-energy absorption coefficients of the red bone marrow and compact bone at a given photon energy. However, instead of this approach, a more conservative one was employed, a worst-case estimate by multiplying the mean absorbed energy in the bone by 1.12 (see Section 4 of [84]) – the peak value of the linear attenuation coefficient ratio curve – resulting in a slight overestimation of the dose absorbed in the active bone marrow.

*Table 2. Organs defined in the model, with their tissue weighting factor ($w_T$) based on the ICRP 103 [8] recommendations.*

| Organ | $w_T$ | Organ | $w_T$ |
|---|---|---|---|
| Active (red) bone marrow | 0.12 | Oral mucosa | 0.12/14 |
| Adrenals | 0.12/14 | Ovaries (Gonads) | 0.08 |
| Bone surface | 0.01 | Pancreas | 0.12/14 |
| Brain | 0.01 | Prostate | 0.12/14 |
| Breast | 0.12 | Salivary glands | 0.01 |
| Colon | 0.12 | Skin | 0.01 |
| Extrathoracic tissue | 0.12/14 | Small intestine | 0.12/14 |
| Gall bladder | 0.12/14 | Spleen | 0.12/14 |
| Heart | 0.12/14 | Stomach | 0.12 |
| Kidneys | 0.12/14 | Testes (Gonads) | 0.08 |
| Liver | 0.04 | Thymus | 0.12/14 |
| Lungs | 0.12 | Thyroid | 0.04 |
| Lymph nodes | 0.12/14 | Urinary bladder | 0.04 |
| Muscle | 0.12/14 | Uterus/cervix | 0.12/14 |
| Oesophagus | 0.04 | | |

Remainder tissues include the adrenals, extrathoracic tissue, gall bladder, heart, kidneys, lymphatic nodes, muscle, oral mucosa, pancreas, small intestine, spleen, thymus, furthermore the sex-specific organs: the prostate and the uterus/cervix, among which the assumed $w_T = 0.12$ is divided evenly (0.12/14).

It is not feasible to model each lymph node of the lymphatic system using quadric geometry. To estimate the absorbed dose to the lymph nodes, selected organs' mean absorbed dose was weighted and summed, with the same weights as used by PCXMC [84]. For the sake of clarity, the following table (Table 3) contains the weights for the estimation of the lymph nodes' mean organ absorbed dose.

*Table 3. Organs and their corresponding weight for the calculation of the mean organ absorbed dose of the lymph nodes. Each of these weights shall be multiplied by the corresponding organ's (or the total body's)* $D_{organ}$ *and summed up to estimate* $D_{lymph\ nodes}$.

| Organ | Weight | Organ | Weight | Organ | Weight |
|---|---|---|---|---|---|
| Small intestine | 0.25 | Salivary glands | 0.08 | Oesophagus | 0.04 |
| Pancreas | 0.15 | Lungs | 0.07 | Heart | 0.04 |
| Extrathoracic tissue | 0.13 | Thyroid | 0.05 | Stomach | 0.03 |
| Gall bladder | 0.1 | Total body | 0.05 | Testes (Gonads) | 0.01 |

The effective dose ($ED$) was calculated according to the recommendations of the ICRP [8], using the following equation (eq. (6)):

$$ED = \sum_{T} w_T D_{organ} \tag{6}$$

where the radiation weighting factor is omitted as its value is 1 for photon radiations and $w_T$ denotes the tissue weighting factor from Table 2.

LAR was calculated for both cancer incidence and mortality. The basis for these metrics is described in detail in the report by the Committee on the Biological Effects of Ionising Radiation [90], Annex 12D. The cited "BEIR VII" report provides two tables for age- and sex-specific risk estimates, Table 12D-1 for cancer incidence and Table 12D-2 for cancer mortality. These were then used to estimate the LAR by simply linearly interpolating between the ages at the time of exposures to find values for cancer incidence and mortality by cancer site (organ). These tables were calculated for a single exposure of 100 mGy of each organ, thus the values were proportionally adjusted for the sum of $D_{organ}$ from each patient's exposures. It is assumed that the expected lifetime (attainable age) of Hungarians does not differ significantly from the one determined for the population of the United States of America. The BEIR VII LAR model uses a dose and dose rate effectiveness factor of 1.5 for each cancer site, except for leukaemia, where a linear-quadratic relationship is established.

### 3.3. Comparative assessment of DVA and DSA

The statistical analysis of the DICOM data obtained in a clinical study bears significant importance. Thus, this section describes the common statistical tests for both the PAD and PAE studies. Depending on the focus of the research at hand, different parameters should be selected for evaluation, thus further subsections concerning each study ensue (3.3.1 for PAD and 3.3.2 for PAE). Throughout the presented studies it was investigated whether the imaging procedures of the two groups were comparable based on several factors, including each patient's total, FLU and SA KAP, along with the current-time product, the tube current, the pulse width, tube voltage, added filtration, field size, total number of frames for each type of image acquisition, age, weight and body mass index. Any change in these may introduce procedural bias, or may show that the goal, namely the reduction of the tube output, has been achieved.

It is important to emphasise that the imaging protocol (overly simplifying it, the target dose rate settings of the image receptor) influences all parameters to be assessed. The total KAP of any procedure is affected by several factors, mainly by the given patient's habitus (single irradiations) and clinical conditions (total time). The former is affected in turn by all parameters mentioned above. The total number of pulses for image acquisition also affects the KAP. Any bias between the two groups would mean that they were treated or selected differently which could be revealed by the appropriate statistical tests. As an example, procedural bias is observable if one group had slightly different handling or had other factors influencing imaging, such as differing field sizes, number of images in a series or differing angulation of the X-ray tube. The Mann-Whitney U-test was used to find out if there is a significant difference between such indicators for each group and further evaluation of bias was done by using the chi-square test. This statistical non-parametric rank test was used, after it was shown that the data cannot be treated as normally distributed. The statistical data were processed with JASP (v0.18.3) and Orange Data Mining (v3.38).

#### 3.3.1 PAD procedures' evaluation

Throughout the clinical study for the comparison of DVA and DSA, an image acquisition protocol with reduced dose was used for patients undergoing the PAD diagnostic procedure with DVA for the angiographic imaging ("Extr. 4 CARE"), while

DSA patients were diagnosed using the protocol with regular dose ("Extr. 2 CARE"). Clinical data are further elaborated by Sótonyi et al. [63]. Further statistical analysis was conducted as outlined in Section 3.3.

### 3.3.2 PAE procedures' evaluation

Both ND and ULD image acquisition protocols were used for the patients undergoing PAE (35 for each protocol). The Fisher's exact test was used to test differences in patient characteristics (age, height, weight, BMI, abdominal diameter, prostate volume), while the Mann-Whitney U-test was used to check bias in procedural aspects of the PAE procedures. During their treatments, the only assumed difference was in the radiological parameters' target settings among the ND and ULD groups.

Different statistical tests were utilised to evaluate the 5-point ordinal scores of raters for DSA and DVA image pairs from three experienced IR specialists, resulting in 210 individual comparisons for PAE. The categories of evaluation were the visualisation of large vessels, small vessels, tissue blush and noise. The scale for diagnostic image quality consisted of: (1) non-diagnostic; (2) poor, with significant limitations; (3) average, allowing for adequate interpretation; (4) good; and (5) excellent visualization with optimal clarity. Additionally, artifacts were evaluated on a similar five-point scale: (1) severe; disabling image interpretation (2) noticeable; moderately affecting the accuracy of image interpretation, (3) moderate; visible but not substantially impacting image reading, (4) minimal; allowing for good image interpretation, (5) no visible; perfect for image reading. An additional option was available, if the structure was not present (for some cases of tissue blush). Only those images were included, which were recognized and scored by all three raters.

Two types of image-quality comparisons were performed. First, DSA and DVA were compared within the same patient group (ND or ULD) to quantify the potential image enhancement achieved by DVA. Second, ND-DSA was compared with ULD-DVA to assess whether DVA could feasibly replace DSA in order to reduce risks from the procedure. The former analysis employed correlated structure statistical methods, whereas the latter required independent group structure approach. High interrater agreement is essential, as the credibility of the results fundamentally depends on it. For interrater association of the samples from the same groups, Kendall's Tau-b was the most

appropriate choice, whereas Bangdiwala's B statistic [91] provided the best assessment for the evaluation of agreement between raters, as detailed below. Bangdiwala's B statistic was used to evaluate interrater agreement. Due to the high level of agreement among raters, the traditional Cohen's kappa paradoxically resulted in a biased estimate, meaning unsatisfactory discord among the ratings, contrary to the obviously observable concordance of raters. Kendall's rank correlation coefficient, here Tau-b which is tie-corrected, was calculated to establish independence of ratings. The Kendall Tau-b statistical test measures the level of agreement among raters on a pair of DVA-DSA image if one or the other is scored better. The Kendall Tau-b coefficient for these comparisons was chosen over other measures due to its suitability for ordinal data and its smaller sensitivity to imbalances in prevalence and marginal distributions.

The ND-DSA and ULD-DVA protocols were also compared by the mean and standard error of the ratings. The significance of the results was assessed with the Mann-Whitney U-test. An interrater Spearman correlation test was employed to demonstrate consistency of ratings. The Spearman test also evaluates the tendency of raters' relative preference by giving a metric on the correlation of their scores. It is less robust if there are many ties in the ratings, but it is relative and can suppress raters' bias. A simple statistical evaluation was done by comparing scores from the raters (DVA preferred, no difference is observed, DSA preferred).

### 3.4. Objective image quality assessment

An IQTO was developed which features a rotating insert [92]. This insert has differing thicknesses of aluminium plates (0.05, 0.1, 0.2 and 0.4 mm) and the stationary part of the test device has copper plates of increasing thickness (0.2 to 1.4 mm in 0.2 mm steps) providing attenuation to imitate the anatomical background. There two 0.2 mm thick copper plates at each end can be used for sanity check or consistency. The insert rotates under or above the stationary part, while the attenuating properties are exactly the same as of the worldwide standardised IQTOs [57–59]. The thickness of the attenuating materials present in the phantom are derived based on the target contrast rate for an ideal imaging system. The rotating insert's aluminium sections create a small contrast difference with the copper during SA and this can demonstrate the contrast enhancement capabilities of DVA through an image series. An image of the test device is shown below (Fig. 6).

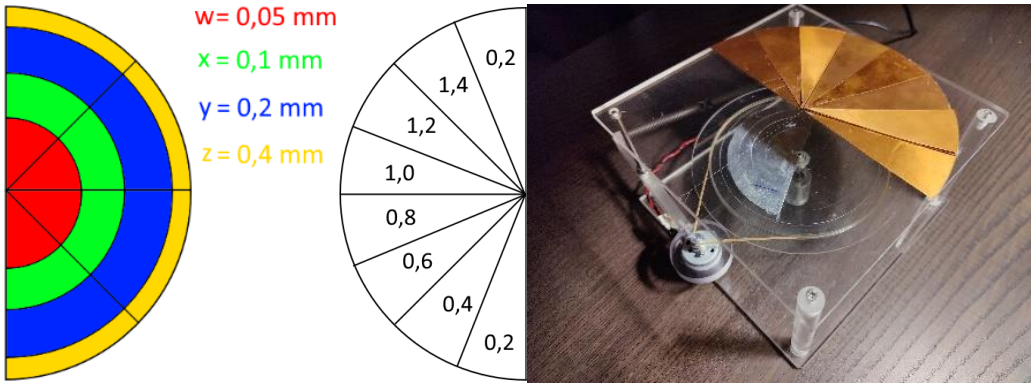


*Fig. 6. Test device with a rotating insert. From left to right: Colour illustration of the aluminium filters and their thickness on the rotating plate; Illustration of the copper plates on top of the test device, divided into sectors, showing the thickness of each copper sector in mm units (decimal separator: ","); Photograph of the test device.*

The General Electric X-ray unit was used to image the IQTO under different circumstances using AERC (at ≈ 58 kVp without significant changes). Different dose settings (100% and 50% target dose rate modes), frame generation frequency (0.5; 1; 2; 4; 7.5 fps), 4 different settings for the rotation speed of the insert (approximately 128, 100, 56 and 40 revolutions per minute - rpm) and three types of image settings were used with different number of frames. The rotation speeds can be set to be on a wide range, commensurate with the blood flow rate from 0.67 m/s of the outmost area at 128 rpm (z on Fig. 6 at 5 cm radius) down to 0.04 m/s of the innermost area at 40 rpm (w on Fig. 6). The differing number of frames from SA image series were used to generate the DSA and DVA images as the following: (1) 2 consecutive images; (2) consecutive images acquired during one rotation of the IQTO's insert (ranging from 2 to 16 frames); and (3) a fixed set of 10 consecutive frames and 5 in the case of 0.5 fps. Each image series underwent the calculation of the summed DSA image, where the first image, used as mask, was subtracted from all images and then these were summed. DVA images were calculated by the KMIT software (v5.0.3.856). The resulting DSA and DVA images were evaluated using ImageJ, where regions of interests (ROIs) matched the sectors in the test device discernible by the overlapping regions of the aluminium and copper plates. CNR was chosen as a singular metric, since it is appropriate for to evaluate image quality [93]. The CNR was calculated according to the following equation (eq. (7)):

$$CNR = \left| \frac{MPV_x - MPV_{bkgx}}{\sqrt{SD_x^2 + SD_{bkgx}^2}} \right| \quad (7)$$

where *MPV* is the mean pixel value, *SD* is their standard deviation and *x* denotes a given sector's section, while *bkgx* refers to the corresponding sector's outmost area on the IQTO which was designated as the background ROI (see Fig. 7). ROI sets were drawn in ImageJ and the measured results from these were then exported to Microsoft Excel for evaluation.

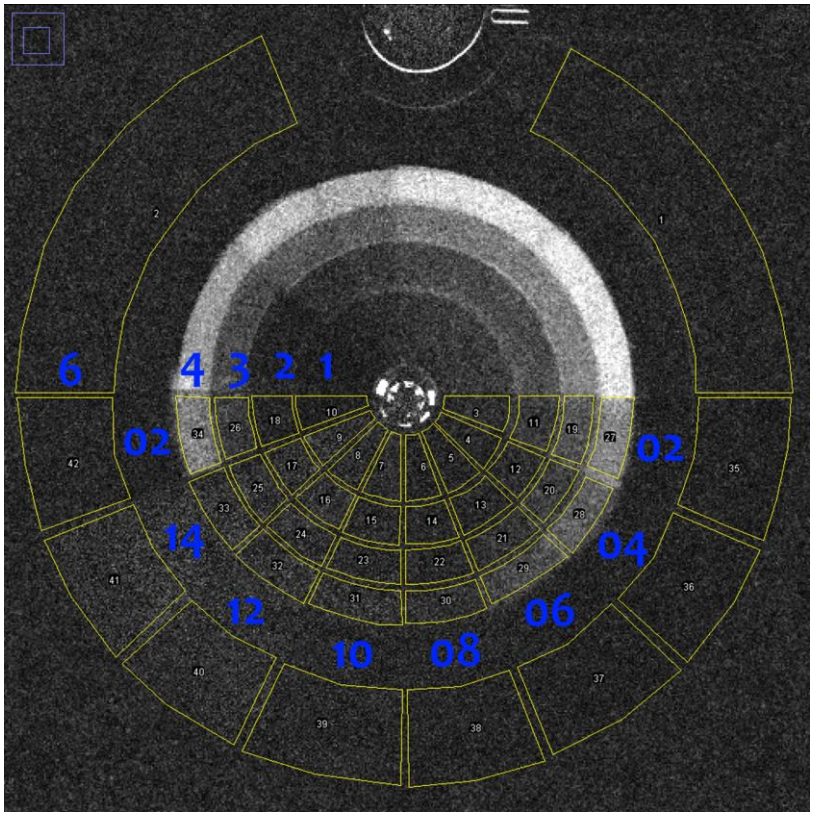


*Fig. 7. An X-ray image of the test object with a rotating insert, showing the different ROIs. Notations 02…14 in the circular pattern show the thickness of the stationary copper plates' sectors in 0.1 mm units. Copper plates extend beyond the outmost ROIs. Notation 6 denotes the outmost stationary copper plates' section. Notations 1 through 4 denote the innermost (0.05 mm aluminium) and the outmost (0.4 mm aluminium) sections of the circular aluminium plate. The drive may be seen on top of the image.*

# 4. Results

## 4.1. Validation of dosimetric quantities

A brief summary of the validation test is presented in Table 4 and Table 5, restricted to contain only the most significant dose indicator used throughout this work, KAP. The indices *meas* and *disp* designate the measured and displayed values respectively. This applies only to kerma-area product values based on the measurement of incident air kerma.

*Table 4. Relative difference in KAP values for the Siemens Artis Zee Floor unit.*

| Series ID | $KAP_{meas}$ (μGym$^2$) | $KAP_{disp}$ (μGym$^2$) | Difference in KAP (%) $(KAP_{meas}-KAP_{disp})/KAP_{meas}$ |
|---|---|---|---|
| S1 | 1.13 | 1.19 | -5.3% |
| S2 | 1.58 | 1.53 | 3.5% |
| S3 | 22.06 | 22.51 | -2.0% |
| S4 | 29.68 | 29.65 | 0.1% |
| S5 | 29.91 | 29.90 | 0.0% |
| S6 | 3.39 | 3.36 | 0.9% |
| S7 | 1.32 | 1.26 | 4.5% |

*Table 5. Difference in KAP values for the GE Innova IGS 540 unit.*

| Series ID | $KAP_{meas}$ (μGym$^2$) | $KAP_{disp}$ (μGym$^2$) | Difference in KAP (%) $(KAP_{meas}-KAP_{disp})/KAP_{meas}$ |
|---|---|---|---|
| S1 | 16.09 | 15 | 6.8% |
| S2 | 16.16 | 16 | 1.0% |
| S3 | 34.63 | 34 | 1.8% |
| S4 | 34.56 | 34 | 1.6% |
| S5 | 34.80 | 34 | 2.3% |
| S6 | 34.46 | 34 | 1.3% |
| S7 | 73.05 | 72 | 1.4% |

The estimated associated uncertainty of the above results is ± 11.7% (k = 2).

## 4.2. Risk assessment of angiographic procedures

### 4.2.1 PAD procedures' risk assessment

The group which was examined with DSA received a CED of 194.7 man×mSv, while the other one for which DVA was utilised, has received 42% of this, 82.6 man×mSv. The CED in the DVA group has been reduced by 58% in this study. Table 6 summarises the LAR estimates for PAD.

*Table 6. Mean LAR cancer incidence and mortality for DVA versus DSA in PAD procedures based on the BEIR VII methodology. The least and most significant ratios of each and reduction rates are underlined.*

| | Site | DSA | DVA | Ratio | Reduction rate | | Site | DSA | DVA | Ratio | Reduction rate |
|---|---|---|---|---|---|---|---|---|---|---|---|
| **LAR (lifetime attributable risk) for cancer incidence per 100 000 cases** | **Stomach** | 2.62E+00 | 1.31E+00 | 50% | 50% | **LAR (lifetime attributable risk) for cancer mortality per 100 000 cases** | **Stomach** | 1.51E+00 | 7.37E-01 | **49%** | **51%** |
| | **Colon** | 3.48E+00 | 1.45E+00 | 42% | 58% | | **Colon** | 1.85E+00 | 7.69E-01 | 42% | 58% |
| | **Liver** | 2.26E-01 | 1.04E-01 | 46% | 54% | | **Liver** | 1.40E-01 | 5.62E-02 | 40% | 60% |
| | **Lung** | 4.06E-01 | 1.75E-01 | 43% | 57% | | **Lung** | 4.26E-01 | 1.81E-01 | 42% | 58% |
| | **Bladder** | 4.24E+00 | 1.24E+00 | 29% | 71% | | **Bladder** | 1.27E+00 | 3.68E-01 | 29% | 71% |
| | **Thyroid** | 5.18E-05 | 1.72E-05 | 33% | 67% | | - | - | - | - | - |
| | **Breast** | 2.79E-02 | 2.09E-02 | **75%** | **25%** | | **Breast** | 2.92E-03 | 1.15E-03 | 39% | 61% |
| | **Uterus** | 5.41E-01 | 1.35E-01 | **25%** | **75%** | | **Uterus** | 5.30E-02 | 8.48E-03 | **16%** | **84%** |
| | **Ovaries** | 3.28E-02 | 8.30E-03 | **25%** | **75%** | | **Ovaries** | 8.14E-03 | 1.29E-03 | **16%** | **84%** |
| | **Prostate** | 1.27E+00 | 3.58E-01 | 28% | 72% | | **Prostate** | 2.75E-01 | 9.29E-02 | 34% | 66% |
| | **Other** | 2.33E+01 | 9.45E+00 | 41% | 59% | | **Other** | 1.41E+01 | 5.68E+00 | 40% | 60% |
| | **All solid** | 3.54E+01 | 1.40E+01 | 40% | 60% | | **All solid** | 1.97E+01 | 7.90E+00 | 40% | 60% |
| | **Leukemia** | 2.12E+00 | 8.37E-01 | 40% | 60% | | **Leukemia** | 1.97E+00 | 7.68E-01 | 39% | 61% |
| | **All cancers** | 3.75E+01 | 1.49E+01 | 40% | 60% | | **All cancers** | 2.16E+01 | 8.67E+00 | 40% | 60% |

Ratio is calculated as $\frac{\mathrm{LAR}_{DVA}}{\mathrm{LAR}_{DSA}}$; Reduction rate is calculated as $\frac{\mathrm{LAR}_{DSA}-\mathrm{LAR}_{DVA}}{\mathrm{LAR}_{DSA}}$.

### 4.2.2 PAE procedures' risk assessment

The ND group received a CED of 229.8 man×mSv, while the ULD group has received 21.5% of this, 49.3 man×mSv. The CED in the ULD group has been reduced by 78.5%. Table 7 summarises the results on LAR, highlighting the organs exposed to higher risk.

*Table 7. Mean LAR cancer incidence and mortality for ULD and ND groups in PAE procedures based on the BEIR VII methodology. The least and most significant ratios of each and reduction rates are underlined. Since this procedure involves the in-field irradiation of the bladder and the prostate, these are also highlighted.*

| | Site | ND | ULD | Ratio | Reduction rate | | Site | ND | ULD | Ratio | Reduction rate |
|---|---|---|---|---|---|---|---|---|---|---|---|
| **LAR (lifetime attributable risk) for cancer incidence per 100 000 cases** | **Stomach** | 1,38E-01 | 1,17E+00 | 12% | 88% | **LAR (lifetime attributable risk) for cancer mortality per 100 000 cases** | **Stomach** | 7.83E-02 | 6.63E-01 | 12% | 88% |
| | **Colon** | 2,00E+00 | 1,12E+01 | 18% | 82% | | **Colon** | 1.13E+00 | 6.11E+00 | 18% | 82% |
| | **Liver** | 2,56E-02 | 3,18E-01 | **8%** | **92%** | | **Liver** | 1.65E-02 | 1.84E-01 | **9%** | **91%** |
| | **Lung** | 1,62E-02 | 1,10E-01 | 15% | 85% | | **Lung** | 1.79E-02 | 1.19E-01 | 15% | 85% |
| | **Bladder** | 4,11E+00 | 1,44E+01 | **29%** | **71%** | | **Bladder** | 1.27E+00 | 4.40E+00 | **29%** | **71%** |
| | **Thyroid** | 3,24E-06 | 1,33E-05 | 24% | 76% | | - | - | - | - | - |
| | **Prostate** | 1,03E+00 | 5,28E+00 | 19% | 81% | | **Prostate** | 4.28E-01 | 2.35E+00 | 18% | 82% |
| | **Other** | 6,29E+00 | 4,06E+01 | 16% | 84% | | **Other** | 3.94E+00 | 2.48E+01 | 16% | 84% |
| | **All solid** | 1,36E+01 | 7,31E+01 | 19% | 81% | | **All solid** | 6.87E+00 | 3.86E+01 | 18% | 82% |
| | **Leukemia** | 1,91E+00 | 8,43E+00 | 23% | 77% | | **Leukemia** | 1.83E+00 | 7.80E+00 | 23% | 77% |
| | **All cancers** | 1,55E+01 | 8,15E+01 | 19% | 81% | | **All cancers** | 8.70E+00 | 4.64E+01 | 19% | 81% |

Ratio is calculated as $\frac{\mathrm{LAR}_{ULD}}{\mathrm{LAR}_{ND}}$; Reduction rate is calculated as $\frac{\mathrm{LAR}_{ND}-\mathrm{LAR}_{ULD}}{\mathrm{LAR}_{ULD}}$.

*The results presented in Section 4.2.2 are not published yet.*

## 4.3. Comparative assessment of DVA and DSA

### 4.3.1 PAD procedures' evaluation

In the PAD study, the DSA group had 53 (36 male), while the DVA group had 54 (44 male) patients. The statistical analysis revealed that there was no procedural bias among the two patient groups, both groups were handled in the same manner by the medical staff. There were no biases in the procedure in terms of the cohorts' characteristics ($p > 0.05$).

The analysis of the procedural data revealed no evidence of bias that would indicate different treatment of each group. The figures related to FLU did not differ significantly for the two groups (total FLU KAP was $p = 0.744$; total FLU time was $p = 0.943$; mean FLU tube current was $p = 0.879$). In fact, these parameters can be deemed as the same according to the Mann-Whitney U-test ($p > 0.05$) and pertinent to the FLU imaging or the whole procedure, the tube voltage, added filtration, field size, total number of pulses, number of image series did not differ significantly.

A total of 2548 image series were produced, of which fluoroscopies were 1001 for the DSA group and 969 for the DVA group, while SA were 291 for the DSA group and 287 for the DVA group.

One notable finding, however, is the significantly different mean pulse width ($p < 0.001$) which is due to its aggressive reduction for the DVA group (94.2 ms mean reduced to 27.0 ms) by the AERC and the slight increase in tube current (369.0 mA for DSA to 430.4 mA for DVA). These resulted in an overall reduction of the total current-time product for the SA imaging (reduced to 36%). This becomes evident by comparing the SA's median KAP for DSA ($4.76\times10^{-4}$ $Gym^2$) and DVA ($1.91\times10^{-4}$ $Gym^2$).

### 4.3.2 PAE procedures' evaluation

The Fisher's exact test confirmed no significant differences between the groups regarding patient characteristics ($p = 0.84$). The mean cumulative KAP from SA was 2 872 ± 396 (mean ± SD) $\mu Gym^2$ in the ND group and 580 ± 66 $\mu Gym^2$ in the ULD group (Mann-Whitney U-test $p < 0.001$), which represents 80% reduction in KAP. Similar reduction was observed in the median and interquartile range values (ND group: 2 052 (3 631) $\mu Gym^2$; ULD group 479 (747) $\mu Gym^2$). There was no difference in the KAP values of FLU imaging. Comparing the ND with ULD acquisitions' hardware settings, as a result from decreasing the target detector dose in the acquisition protocols, the mean kVp was reduced slightly from 84 kV to 76 kV, while the mean added copper filtration became larger from 0.298 mm to 0.709 mm. The mean tube current also decreased from 321 mA to 242 mA.

Procedural differences for the ND and ULD groups are insignificant, as the number of series ($p = 0.334$), the total number of pulses ($p = 0.601$) and the mean of total exposure times ($p = 0.089$) were not significantly different based on the Mann-Whitney U-test for the ULD and ND groups. However, the total KAP ($p = 0.001$) and the mean dose per pulse ($p = 0.001$) for these groups are significantly different, based on the same test.

For interrater agreement, the Bangdiwala's B values evaluation is summarized in Table 8. The Mann-Whitney U-test showed that raters A, B, and C agreed that ND-DVA and ULD-DVA provided better visualization of large and small vessels, as well as tissue blush, compared to DSA ($p < 0.001$). However, for background noise, the results varied ($p = 0.047$ for rater A, 0.002 for B, and 0.085 for C).

*Table 8. Bangdiwala's B values representing the pairwise interrater agreement among the three raters, calculated for each evaluation criteria of images recorded using the ND (top) and ULD (bottom) protocols. Concordance is also interpreted and categorised as recommended by [91].*

| **ND imaging protocol** | | | | |
|---|---|---|---|---|
| | **Large vessels** | **Small vessels** | **Tissue Blush** | **Noise** |
| **Rater A vs Rater B** | 0.548 (substantial) | 0.734 (almost perfect) | 0.476 (substantial) | 0.309 (moderate) |
| **Rater A vs Rater C** | 0.244 (moderate) | 0.199 (moderate) | 0.243 (moderate) | 0.181 (moderate) |
| **Rater B vs Rater C** | 0.384 (substantial) | 0.401 (substantial) | 0.480 (substantial) | 0.318 (moderate) |
| **ULD imaging protocol** | | | | |
| | **Large vessels** | **Small vessels** | **Tissue Blush** | **Noise** |
| **Rater A vs Rater B** | 0.427 (substantial) | 0.558 (substantial) | 0.492 (substantial) | 0.523 (substantial) |
| **Rater A vs Rater C** | 0.290 (moderate) | 0.361 (substantial) | 0.342 (moderate) | 0.425 (substantial) |
| **Rater B vs Rater C** | 0.345 (moderate) | 0.528 (substantial) | 0.527 (substantial) | 0.626 (substantial) |

The Spearman test showed a strong correlation in all pairwise comparisons of raters' evaluations of large and small vessels and tissue blush ($p < 0.001$) for both ND and ULD acquisitions. However, no correlation was found for background noise ratings between raters A and B ($p = 0.643$) or A and C ($p = 0.166$) in ND images, while a moderate correlation was observed between raters B and C ($p = 0.033$). For ULD images, background noise ratings showed strong correlations across all rater comparisons ($p < 0.001$ for A-B, $p = 0.015$ for A-C, and $p = 0.015$ for B-C). For both ND and ULD ratings, raters showed strong agreement on large and small vessels and tissue blush ($p < 0.001$). For background noise in the ND-DSA dataset, disagreement was observed ($p = 0.640$ for rater A-B, 0.161 for A-C, and 0.036 for B-C). In contrast, ULD-DVA ratings showed strong agreement between raters A and B ($p < 0.001$), with slight disagreement between A-C and B-C (both $p = 0.016$).

For large vessels, the mean score (mean ± SD from hereon) for ND-DVA ($2.94 \pm 0.14$) was significantly higher than ND-DSA ($1.94 \pm 0.088$), while ULD-DVA

(3.03 ± 0.136) also exceeded ULD-DSA (2.00 ± 0.10). Similar trends were observed for small vessels, where ND-DVA (3.98 ± 0.10) and ULD-DVA (4.11 ± 0.09) achieved notably higher scores compared to ND-DSA (2.88 ± 0.08) and ULD-DSA (3.03 ± 0.08) ($p < 0.001$). Tissue blush also demonstrated a marked difference, with ND-DVA (2.41 ± 0.12) and ULD-DVA (2.79 ± 0.10) scored significantly better than ND-DSA (1.58 ± 0.08) and ULD-DSA (1.84 ± 0.08) ($p < 0.001$). For background noise, while ND-DVA (3.83 ± 0.08) and ULD-DVA (3.93 ± 0.06) still outperformed ND-DSA (3.73 ± 0.06) and ULD-DSA (3.00 ± 0.07), the differences were less pronounced. Fig. 8 illustrates a strong rater preference for DVA over DSA across all categories and dose levels when the scores for each series are directly compared. For ND-DVA, readers consistently rated it superior for the visualisation of large vessels (116 cases), small vessels (144 cases), tissue blush (103 cases), and noise (61 cases), compared to ND-DSA (21, 12, 21, and 36 cases, respectively). Similarly, ULD-DVA received higher ratings for large vessels (118 cases), small vessels (148 cases), tissue blush (112 cases), and noise (150 cases), significantly outperforming ULD-DSA (17, 11, 14, and 8 cases, respectively).

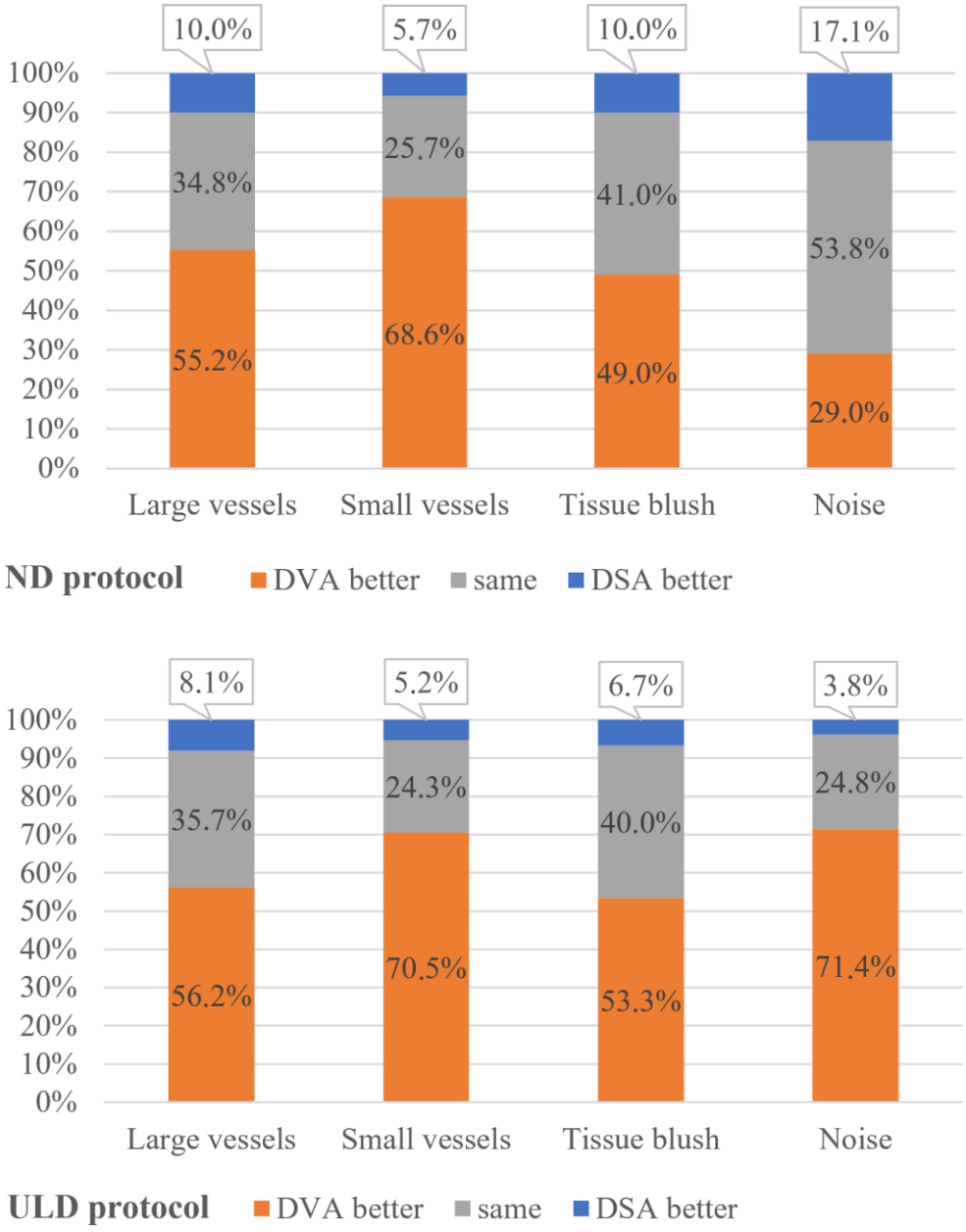


*Fig. 8. Stacked column charts illustrating the qualitative preference of the 3 raters for image quality across four evaluation categories: large vessels, small vessels, tissue blush, and background noise. The plot compares the qualitative preference of each rater between the imaging datasets from normal dose (ND, upper panel) and ultra-low dose (ULD, bottom panel) imaging protocols with DVA (orange) and DSA (blue) image processing. Instances where no difference was observed are labelled as "same" with grey colour.*

### 4.4. Objective image quality assessment

The image quality phantom was evaluated by calculating all of the summed DSA images and the DVA images generated by the KMIT, then each set of results were compared for the same machine settings according to the above-described methodology. All (10 800) data points were checked by comparison for similar rotations speed, image number and frame rate settings. Where more than two images were used for the DVA and DSA image generation, the CNR calculated for ROIs of larger contrast differences (e.g., 0.4 mm aluminium under 0.2 mm copper) shown that the CNR of DVA images are always larger in these regions than those of DSA image sets. The extent of this enhancement can be up to about a factor of 3 in the case of DVA vs. DSA compared at the same dose level, with more than two images, where details would be discernible at all for a human observer (CNR ≈ 1.5). The following figure is illustrative of the results (Fig. 9).

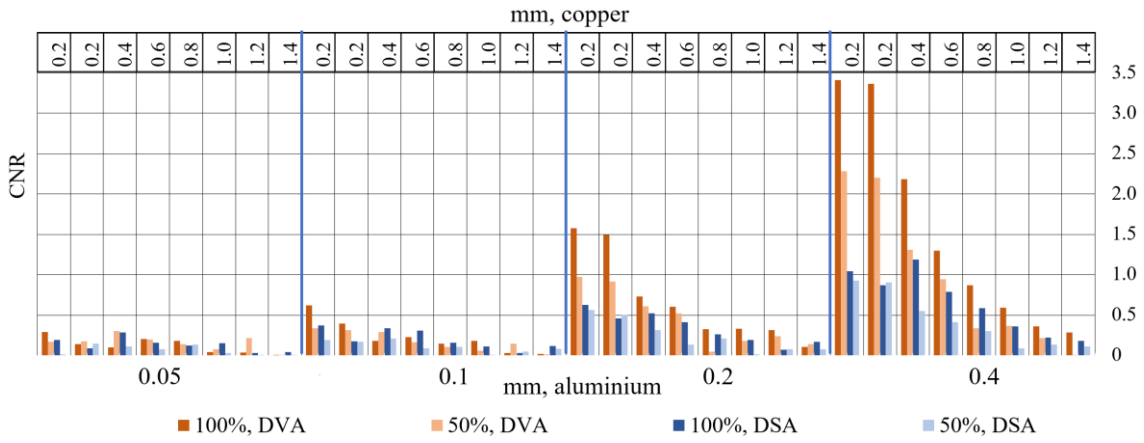


*Fig. 9. An example of the results' comparison; here: 128 rpm, 10 images, 2 frames per second. The vertical axis shows the CNR as described in Section 3.4. Values of CNR are aligned to the right for visual fidelity. The IQTO's sections where the copper plates are the thinnest (0.2 mm) are displayed by each other.*

# 5. Discussion

## 5.1. Validation of dosimetric quantities

Both X-ray units tested provided a reliable indication of the displayed dosimetric quantities. Uncertainty is largely due to the perceived source location and the inherent uncertainty of traceability.

One notable thing is that the relative uncertainty's largest component becomes the digit error of the displayed dosimetric quantity, if it is very small. This is due to the digits which could be resolved, calculated or measured and stored by the given angiographic system. If the air kerma at the interventional reference point is in the order of a few μGy, this effect is significant. In practice, this is the case for very short fluoroscopic exposures, but these are out of interest for the present studies, as only SAs are considered and these are carried out with considerably higher air kerma rates.

Regular quality control tests are a requirement and an indispensable tool for the consistent and reliable operation of angiographic machines and radiological equipment [51,81]. Verification of dosimetric indicators is essential when clinical studies and research are conducted on equipment using ionising radiation.

## 5.2. Risk assessment of angiographic procedures

The two clinical studies included in this thesis are not biased by variations in care provided by the IR specialists. There is a marked difference only for the KAP values in both studies due to the reduced target dose rates, as planned in the study designs. The larger the imaged object is, the more X-rays are required to achieve the target image quality, as determined by the AERC system of the angiographic unit. There are several parameters influencing the quality and quantity of X-rays, but parameters listed in Section 3.3 were mostly not influenced by the choice of the image acquisition protocol, except for the metrics determining the quality and quantity of radiation.

The methodology of quadric geometry phantom based MC simulations to determine the organ absorbed doses has certain limitations to be noted. This approach relies on a basic geometrical model and does not incorporate more advanced techniques such as computer-aided design patient models or phase space data for the X-ray radiation field, etc. Furthermore, the approach to estimating the mean absorbed dose to the bone marrow is conservative, potentially leading to an overestimation of both the absorbed dose to the

bone marrow and the slight overestimation of the ED. However, since this methodology is consistently applied to every patient group, it does not introduce bias into the comparative analyses, thereby maintaining the integrity of the studies as a benchmark investigation of ED and LAR.

The use of ED and CED of the radiation exposure of the patients undergoing PAD procedures is an indicator of radiological risks in the presented studies. The CED enables the benchmarking of the efficacy of DVA against the standard DSA image processing and serves as a guide for optimisation [94,95]. ED uses many approximations, but its present use as CED falls within the defensible scope [96,97] of its utility for the characterisation of medical exposures as two similar group of patients were included in each study. Risk-related metrics for low doses of ionising radiation are scarce, thus the BEIR VII methodology [44,90,98] was adapted. This leans heavily on expert agreement and since the effects of low doses of ionising radiation is not fully understood, the presented numerical data requires care when interpreted and communicated. This is partly due to misinterpretation and results may be sensationalised. Baseline lifetime risk estimates of cancer incidence and mortality are present in the Committee's publication (see Table 12-4), corresponding to about 20% baseline risk of cancer mortality and around double this figure for cancer incidence. Accounting for the baseline cancer risks, the dose saving may seem miniscule, however when we consider the latest UNSCEAR report [13] on the ever increasing frequency of angiographic procedures worldwide, the benefit of DVA may be translated into potential cost-effectiveness due to the averted risk [99]. The BEIR VII model has high uncertainties associated with it [100] and readers must keep in mind that the study was limited to low doses where the model is an extrapolation from the available data for high dose exposures. To illustrate the extent of uncertainty associated with the LAR model, the BEIR VII commission provides a set of subjective uncertainties in their report (Table 12-5A) [90] for mixed ages which are a factor of two to three, but can be as high as one order of magnitude. A simpler approach would be to use the ICRP 103 [8] recommendation on the risk coefficient of 5%/Sv, which is a sex- and age averaged figure, yielding similar ratios for the groups, but a larger value in terms of absolute risk based on the groups' CED.

For neither of the clinical studies have deterministic effects been considered. To justify this consideration, the level of radiation exposure would not be enough to trigger

even the slightest skin reaction in the populations being investigated. Deterministic effects, however, may arise due to complex procedures [101–104]. Using DVA instead of the traditional DSA may be helpful to reduce radiological risks in any interventional procedure. Several clinical studies have already provided evidence supporting this [34,38,40], indicating that the use of DVA may also help avoiding skin injuries.

PAE procedures are more complicated in clinical terms and are concentrated around highly radiosensitive organs, the bladder, the prostate and partially the colon. Slight bias in the organs or their characteristics and positions may influence the direct translation of physical dose metrics into cancer risk. This effect is insignificant in a statistical sense as bias was not shown among any of the corresponding patient groups but the presence of women slightly biased LAR for the PAD study. High organ specific absorbed doses to highly radiation sensitive organs result in a larger cancer risk to patients. This effect is blurred by the use of a singular, more simple metric, ED or CED. Stochastic risks also extends to medical staff, especially in high-volume PAE centers [105–107].

These findings are pertinent to SA. Depending on the complexity of the angioplasty or radio- and chemoembolisation procedures, SAs may be a large contributor to the dose indices of the overall procedure. Such procedures may pose higher overall radiological risks than PAE [18–20] and repeat procedures should be considered as well, which may elaborate DVA's indispensability. These may be in the focus of future research.

Medical exposures cannot be limited in the same way as radiological protection would approach other exposure categories' risk management. With the risk averting feature of DVA, repeat procedures should have a better risk-benefit balance. This may fall in the scope of further studies. The framework to estimate risk from interventional procedures can be enhanced and amended to be applicable for any radiological procedure.

With regular quality control tests, the modern angiography units and most radiological imaging devices can provide reliable data for dose monitoring systems and this data could be fed into the risk assessment framework. Elements for the evaluation of a skin dose map is already implemented in the risk assessment framework, but fell out of the scope of the presented studies, nonetheless it bears clinical importance [103,108,109]. This would in turn enable raising awareness of radiological risks and help elaborate optimisation efforts carried out by medical physicists and other clinical staff.

### 5.2.1 PAD procedures' risk assessment

The specific study on PAD procedures revealed that a large reduction in physical dose quantities, here highlighting KAP as the indicator, may be achieved by using DVA. This was 60% in this study ($4.76\times10^{-4}$ $Gym^2$ mean for DSA compared to $1.91\times10^{-4}$ $Gym^2$ for DVA). The use of the "Extr. 4 CARE" protocol for DVA in this study, compared to the "Extr. 2 CARE" protocol for DSA provided for much shorter impulse times, a slightly higher current and consequently an overall reduction of the current–time product. This in turn enabled the reduction of kerma-area product for the SA. Using smaller pulse widths for imaging provides a further benefit, as the procedure becomes less prone to apparent motion-related artifacts. The tube current used for the SAs were also different. This is due to the headroom in generator power and cooling due to the smaller tube loading factor.

Overall, with the use of DVA instead of DSA, the cancer risk can be reduced by a factor of 2.5 due to the SAs from PAD procedures.

### 5.2.2 PAE procedures' risk assessment

Targeted embolisation of the prostate is considered more complicated than routine diagnostic angiographic procedures such as PAD. The radiological risk reduction in relative terms is similar to PAD procedures, as 78.5% CED reduction was observed. The risk indices were reduced, LAR cancer incidence by 71% … 92% and by 71% … 91% cancer mortality to a slightly larger extent than for the PAD study.

## 5.3. Comparative assessment of DVA and DSA

The methodological shortcomings as discussed in Section 5.1 are present. However, these do not undermine the veracity of the results obtained for the comparison of the two groups. The methods used to test procedural bias, which may arise from the different handling of the patient groups have revealed that it has not influenced the studies.

The ability of DVA to achieve substantial radiation dose reductions while preserving image quality, positions it as a valuable tool for other angiographic procedures, for treating benign tumours, peripheral vascular disease, or transarterial embolization for myomas or periarticular pain [110]. Moreover, previous studies showed that DVA can reduce contrast agent usage by 50% in carotid angiography [34]. The arbitrary combination of lower radiation and/or contrast media usage suggests potential benefits for both paediatric and other patients at-risk [111,112].

## 5.4. Objective image quality assessment

The underlying technology of KMIT is straightforward. The results obtained with the IQTO align well with the theoretically derivable consequences of how DVA operates [29]. DVA utilises all images and enhances changes in images with moving objects. The more images one feeds to the algorithm, the more effective the contrast enhancement will be. DVA confutes its simplicity by being a valuable tool in IR to strengthen contrast or to reduce the radiation dose while maintaining the same image quality as the currently employed image processing method, DSA.

The specific IQTO is an experimental prototype, which has proven its utility, but would still require further development to be used in clinical suites. After addressing safety issues and hazards which may arise from experimental prototypes, the phantom could be used more conveniently (e.g., with a rechargeable battery, software for automatic evaluation etc.) and since it has the same attenuation features as the currently used standard phantom, it could eventually replace it and still provide comparable results. Another possible use of the IQTO would be the evaluation of motion-related artefacts which were not studied through my work, but may prove to be useful. This study should investigate the relation of rotation speed, contrast media injection, CNR and furthermore the objective assessment of motion blur. The IQTO features an interchangeable insert. The current insert is equivalent in terms of attenuation to the currently accepted standard, but the interchangeability makes it future-proof as an IQTO.

The IQTO developed provides for the evaluation of DVA and a further use for it could be to test KMIT during commissioning and to perform acceptance and status tests at regular intervals. It can be also used to objectively compare different imaging protocols and IR units from different vendors, before and after commissioning a new system.

## 6. Conclusions

DVA enables up to 80% reduction for SA in radiation exposure in complex interventional procedures such as PAE while maintaining diagnostic image quality. While reducing radiation dose, image quality is preserved. This supports DVA's role as a safer alternative to DSA in angiographic procedures.

According to the linear-non threshold model, the reduction of physical dose indices translates into the reduction of associated stochastic and deterministic radiation risks. Dose reduction of the patient draws along the reduction of dose to the staff and costs associated with care, benefiting patient outcome and contribute to sustainable, safe and quality care. Consequently, DVA is a valuable tool to help optimising radiation protection of patients and staff alike and could herald a paradigm shift in angiographic imaging.

Future research should explore the utility of DVA in contrast media use and further validate its benefits in clinical settings and implications for vulnerable patient cohorts.

**Novel, thesis-related findings**

1) I have verified that the dose metrics provided by the angiography units are satisfactory.

2) I have developed a MC particle transport simulation framework which relies on the image metadata from the angiographic procedures.

3) I have demonstrated the utility of this particle transport framework for the risk assessment of PAD and PAE procedures.

    a. With the use of DVA, radiation dose during an exposure may be reduced by up to 80% compared to the otherwise clinically used DSA imaging.

    b. Reduction of the quantities describing physical dose to the patient translates into a decreased risk of cancer incidence by 25% to 75% and cancer mortality by 51% to 84% for PAD procedures depending on the cancer site.

    c. The dose reduction in PAE results in the reduction of 71% to 92% in cancer incidence and 71 to 91% reduction in cancer mortality depending on the cancer site.

4) DVA is superior compared to DSA in subjective and objective image quality evaluations.

   a. I have designed and built a test object to quantitatively evaluate the CNR of DVA and demonstrated that if more than two images are processed by KMIT, DVA has an advantage in terms of CNR compared to summed DSA, by up to a factor of 3.

   b. A randomized controlled trial for PAE revealed that DVA images are superior to DSA for the visualisation of large vessels, small vessels and tissue blush in subjective evaluations of PAE procedures, as DVA achieved significantly higher scores from experienced raters ($p < 0.001$; rating: 3.03 vs 2.00; 4.11 vs 2.88; 2.79 vs 1.58 respectively) under any target dose rates.

## 7. Summary

This thesis investigates the efficacy of Digital Variance Angiography (DVA) and compares it to the prevalent technology, Digital Subtraction Angiography (DSA). The scope includes the radiological risk assessment of Peripheral Artery Disease (PAD) and Prostatic Artery Embolisation (PAE) procedures, complemented with the subjective image quality assessment of the latter. For the objective image quality evaluation of DVA, this work also presents the development of a new test object (IQTO).

For the risk assessment of PAD procedures (54 DVA and 53 DSA patients), the PENELOPE MC particle transport code was adapted. Simulations rely on the image metadata to estimate organ absorbed dose, effective dose and lifetime attributable cancer risk. A prospective randomised controlled trial enrolled 70 patients for PAE with normal dose (ND, 35) and ultra-low dose (ULD, 35). Three experienced radiologists evaluated the visualisation of large vessels, small vessels, tissue blush and background noise of DVA and DSA images on a 5-point ordinal scale. Statistical analysis of ratings included Mann-Whitney U-tests for intragroup comparisons, Spearman correlation for consistency, Kendall Tau-b and Bangdiwala's B for interrater agreement. The radiological risks from PAE were also estimated. For the objective image quality assessment, the development of an IQTO with a rotating insert was required, having the same features as the currently standardised IQTO.

Radiation dose indices and risks were reduced by about 60% for PAD, while it is about 80% for PAE procedures in stationary acquisitions. Subjective visual evaluation from three raters conclusively found that DVA images are favoured for the visualisation of large vessels, small vessels and tissue blush with any dose settings. Consensus was lacking for background noise. The CNR on DVA images made with the new IQTO may be up to 3 times higher than for the summed DSA images.

DVA significantly improves image quality compared to DSA of the procedures included in the presented studies, which allows up to 80% reduction of radiation burden to patients and staff alike, while it also maintains diagnostic image quality.

Future research may focus on the investigation of staff dose reduction, patients at-risk along the potential reduction of contrast media.

**Összefoglaló**

E disszertáció a digitális variancia angiográfia (DVA) hatékonyságát vizsgálja, melyet az uralkodó, digitális szubtrakciós angiográfiával (DSA) hasonlít össze. Felöleli a perifériás artériás betegség (PAD) és a prosztata artériás embolizáció (PAE) eljárásainak radiológiai kockázatelemzését, az utóbbi esetén kiegészítve azt a képminőség vizsgálatával. A DVA objektív képminőség-értékelése érdekében e munka egy új vizsgálótestet (IQTO) fejlesztését is bemutatja.

A PAD eljárások kockázatértékeléséhez (54 DVA és 53 DSA pácienssel), a PENELOPE MC részecsketranszport szimulációs kód kerül felhasználásra. A szimulációk a képi metaadatokon alapszanak a szervben elnyelt dózis, az effektív dózis és az élettartam-társított rákkockázat becsléséhez. 70 páciens bevonásával történt prospektív véletlenített kontrollált vizsgálat a PAE értékelésére normál dózissal (ND, 35) és ultra-alacsony dózissal (ULD, 35). Három tapasztalt radiológus értékelte a nagy erek, a kis erek, a szöveti pír és a háttér zajának megjelenését egy ötpontos sorrendi skálán. Az értékelések statisztikai elemzése az egyes csoportokon belüli értékelésre Mann-Whitney U-teszttel, az értékelések következetességére Spearman-korreláció elemzéssel, az elemzők közti egyetértéshez pedig Kendall Tau-b és Bangdiwala B statisztikával történt. A PAE radiológiai kockázatainak a becslése ugyancsak megtörtént. Az objektív képminőség-értékelés egy forgóbetétes IQTO kifejlesztését igényelte, melynek jellemzői a jelenleg szabványosított képminőség-vizsgáló testével megegyezők.

A radiológiai dózis indikátorok és kockázatok a PAD esetén 60% körüli arányban csökkentek, míg a PAE esetén 80%-nyival az érleképezéskor. A három értékelő egyéni láthatóság-értékelése következetesen azt mutatta, hogy a DVA képek bármely dózisszint mellett előnyösebbek a nagy erek, a kis erek, a szöveti pír megjelenítéséhez. Az ND képalkotáskor nem volt közmegegyezés a háttérzajra. A DVA képek új IQTO-val értékelt kontraszt-zaj aránya akár háromszorosát is elérheti az összegzett DSA képekének.

A DVA jelentősen javítja a képminőséget a DSA-hoz képest a jelen tanulmányokba vont eljárások során, mely lehetővé teszi a páciensek és a személyzet sugárterhelésének akár 80%-nyi csökkentését a diagnosztikai érték fenntartása mellett.

A jövőbeli kutatás összpontosíthat a személyzet dóziscsökkentésére és a magas kockázatú betegekre a kontrasztanyag lehetséges csökkentése révén.

## 8. References


1. Malley MC. Radioactivity: a history of a mysterious science. New York: Oxford University Press; 2011. 290 p.

2. X-Ray and Radium Protection: Recommendations of International Congress of Radiology. Radiology. 1929 June;12(6):519–24.

3. Recommendations of the International X-ray and Radium Protection Commission. Br J Radiol. 1931 Oct;4(46):485–7.

4. International Recommendations for X-Ray and Radium Protection: Revised by the International X-Ray and Radium Protection Commission at the Fourth International Congress of Radiology, Zürich, July 1934. 1934;7.

5. International Recommendations for X-Ray and Radium Protection: Revised by the International X-Ray and Radium Protection Commission at the Fifth International Congress of Radiology, Chicago, September, 1937. 1937;6.

6. Kathren RL. William H. Rollins (1852–1929): X-ray Protection Pioneer. J Hist Med Allied Sci. 1964;XIX(3):287–95.

7. Walker JS. Permissible Dose: A History of Radiation Protection in the Twentieth Century. Berkeley, CA: University of California Press; 2000. 182 p.

8. Valentin J, International Commission on Radiological Protection, editors. The 2007 recommendations of the International Commission on Radiological Protection. Oxford: Elsevier; 2007. 332 p. (ICRP publication).

9. Simeonov G, Mundigl S, Janssens A. Radiation protection of medical staff in the latest draft of the revised Euratom Basic Safety Standards directive. Radiat Meas. 2011 Nov;46(11):1197–9.

10. European Society of Radiology (ESR). Summary of the European Directive 2013/59/Euratom: essentials for health professionals in radiology. Insights Imaging. 2015 Aug;6(4):411–7.

11. Tay YX, Foley SJ, Ong ME, Chen RC, Chan LP, Killeen R, Tan EJ, Mak MS, McNulty JP. Using evidence-based imaging referral guidelines to facilitate appropriate imaging: Are they all the same? Eur J Radiol. 2025 Feb;183:111933.

12. Sources and effects of ionizing radiation: United Nations Scientific Committee on the Effects of Atomic Radiation: UNSCEAR 2008 report to the General Assembly, with scientific annexes. New York: United Nations; 2010. 683 p.

13. Sources, effects and risks of ionizing radiation: UNSCEAR 2020/2021 report to the General Assembly, with scientific annexes. New York: United Nations; 2021. 308 p.

14. Circulatory diseases are Europe's biggest killer. BMJ. 2006 July 29;333(7561):218.3.

15. OECD, European Commission. Health at a Glance: Europe 2024: State of Health in the EU Cycle [Internet]. OECD Publishing; 2024 [cited 2025 Dec 8]. 233 p. (Health at a Glance: Europe). Available from: https://www.oecd.org/en/publications/health-at-a-glance-europe-2024_b3704e14-en.html

16. OECD, European Observatory on Health Systems and Policies, editors. Hungary: Country Health Profile 2023. Paris: OECD Publishing; 2023. 24 p. (State of Health in the EU).

17. European Commission, editor. Medical radiation exposure of the European population. Luxembourg: Publications Office; 2015. 181 p. (Radiation Protection; vol. 1).

18. Jones AK, Wunderle KA, Fruscello T, Simanowith M, Cline B, Dharmadhikari S, Duan X, Durack JC, Hirschl D, Kim DS, Mahmood U, Mann SD, Martin C, Metwalli Z, Moirano JM, Neill RA, Newsome J, Padua H, Schoenfeld AH, Miller DL. Patient Radiation Doses in IR Procedures: The American College of Radiology Dose Index Registry-Fluoroscopy Pilot. J Vasc Interv Radiol. 2023 Apr;34(4):544-555.e11.

19. Miller DL. Review of air kerma-area product, effective dose and dose conversion coefficients for non-cardiac interventional fluoroscopy procedures. Med Phys. 2020 Mar;47(3):975–82.

20. Miller DL. Overview of contemporary interventional fluoroscopy procedures. Health Phys. 2008 Nov;95(5):638–44.

21. Jones AK, Wunderle KA, Fruscello T, Simanowith M, Cline B, Dharmadhikari S, Duan X, Durack JC, Hirschl D, Kim DS, Mahmood U, Mann SD, Martin C, Metwalli Z, Moirano JM, Neill RA, Newsome J, Padua H, Schoenfeld AH, Miller DL. Patient Radiation Doses in IR Procedures: The American College of Radiology Dose Index Registry-Fluoroscopy Pilot. J Vasc Interv Radiol. 2023 Apr;34(4):544-555.e11.

22. Fisher RF, Applegate KE, Berkowitz LK, Christianson O, Dave JK, DeWeese L, Harris N, Jafari ME, Jones AK, Kobistek RJ, Loughran B, Marous L, Miller DL, Schueler B, Schwarz BC, Springer A, Wunderle KA. AAPM Medical Physics Practice Guideline 12.a: Fluoroscopy dose management. J Appl Clin Med Phys. 2022 Mar;23(3):e13526.

23. Clement CH, editor. Diagnostic reference levels in medical imaging. Thousand Oaks, Calif.: SAGE; 2017. 147 p.

24. Balter S, Rosenstein M, Miller DL, Schueler B, Spelic D. Patient radiation dose audits for fluoroscopically guided interventional procedures. Med Phys. 2011 Mar;38(3):1611–8.

25. Jones AK, Balter S, Rauch P, Wagner LK. Medical imaging using ionizing radiation: Optimization of dose and image quality in fluoroscopy: Optimization of dose and image quality in fluoroscopy. Med Phys. 2013 Dec 9;41(1):014301.

26. Radiation Protection and Safety in Medical Uses of Ionizing Radiation. Vienna: International Atomic Energy Agency; 2018. 340 p. (Safety Standards Series).

27. Modarai B, Haulon S, Ainsbury E, Böckler D, Vano-Carruana E, Dawson J, Farber M, Van Herzeele I, Hertault A, Van Herwaarden J, Patel A, Wanhainen A, Weiss S, Esvs Guidelines Committee, Bastos Gonçalves F, Björck M, Chakfé N, De Borst GJ, Coscas R, Dias NV, Dick F, Hinchliffe RJ, Kakkos SK, Koncar IB, Kolh P, Lindholt JS, Trimarchi S, Tulamo R, Twine CP, Vermassen F, Document Reviewers, Bacher K, Brountzos E, Fanelli F, Fidalgo Domingos LA, Gargiulo M, Mani K, Mastracci

TM, Maurel B, Morgan RA, Schneider P. Editor's Choice – European Society for Vascular Surgery (ESVS) 2023 Clinical Practice Guidelines on Radiation Safety. Eur J Vasc Endovasc Surg. 2023 Feb;65(2):171–222.

28. Levin D, Schapiro R, Boxt L, Dunham L, Harrington D, Ergun D. Digital subtraction angiography: principles and pitfalls of image improvement techniques. Am J Roentgenol. 1984 Sept 1;143(3):447–54.

29. Szigeti K, Domokos M, Osvath S. Motion Based X-Ray Imaging Modality. IEEE Trans Med Imaging. 2014 Oct;33(10):2031–8.

30. Osváth S. Honey I shrunk the dose! Poster presented at: 5th European Congress of Medical Physics Joint Conference of the DGMP, ÖGMP & SGSMP; 2024.

31. Gyánó M, Góg I, Óriás VI, Ruzsa Z, Nemes B, Csobay-Novák C, Oláh Z, Nagy Z, Merkely B, Szigeti K, Osváth S, Sótonyi P. Kinetic Imaging in Lower Extremity Arteriography: Comparison to Digital Subtraction Angiography. Radiology. 2019 Jan;290(1):246–53.

32. Óriás VI, Gyánó M, Góg I, Szöllősi D, Veres DS, Nagy Z, Csobay-Novák C, Zoltán O, Kiss JP, Osváth S, Szigeti K, Zoltán R, Sótonyi P. Digital Variance Angiography as a Paradigm Shift in Carbon Dioxide Angiography. Invest Radiol. 2019 July;54(7):428–36.

33. Gyánó M, Csobay-Novák C, Berczeli M, Góg I, Kiss JP, Szigeti K, Osváth S, Nemes B. Initial Operating Room Experience with Digital Variance Angiography in Carbon Dioxide-Assisted Lower Limb Interventions: A Pilot Study. Cardiovasc Intervent Radiol. 2020 Aug;43(8):1226–31.

34. Óriás VI, Szöllősi D, Gyánó M, Veres DS, Nardai S, Csobay-Novák C, Nemes B, Kiss JP, Szigeti K, Osváth S, Sótonyi P, Ruzsa Z. Initial evidence of a 50% reduction of contrast media using digital variance angiography in endovascular carotid interventions. Eur J Radiol Open. 2020;7:100288.

35. Bastian MB, König AM, Viniol S, Gyánó M, Szöllősi D, Góg I, Kiss JP, Osvath S, Szigeti K, Mahnken AH, Thomas RP. Digital Variance Angiography in Lower-Limb

Angiography with Metal Implants. Cardiovasc Intervent Radiol. 2021 Mar;44(3):452–9.

36. Gyánó M, Berczeli M, Csobay-Novák C, Szöllősi D, Óriás VI, Góg I, Kiss JP, Veres DS, Szigeti K, Osváth S, Pataki Á, Juhász V, Oláh Z, Sótonyi P, Nemes B. Digital variance angiography allows about 70% decrease of DSA-related radiation exposure in lower limb X-ray angiography. Sci Rep. 2021 Nov 8;11(1):21790.

37. Thomas RP, Bastian MB, Viniol S, König AM, Amin SS, Eldergash O, Schnabel J, Gyánó M, Szöllősi D, Góg I, Kiss JP, Osváth S, Szigeti KP, Mahnken AH. Digital Variance Angiography in Selective Lower Limb Interventions. J Vasc Interv Radiol. 2022 Feb;33(2):104–12.

38. Alizadeh LS, Gyánó M, Góg I, Szigeti K, Osváth S, Kiss JP, Yel I, Koch V, Grünewald LD, Vogl TJ, Booz C. Initial Experience Using Digital Variance Angiography in Context of Prostatic Artery Embolization in Comparison with Digital Subtraction Angiography. Acad Radiol. 2023 Apr;30(4):689–97.

39. Alizadeh LS, Gyánó M, Góg I, Szigeti K, Osváth S, Kiss JP, Yel I, Koch V, Grünewald LD, Vogl TJ, Booz C. Initial Experience Using Digital Variance Angiography in Context of Prostatic Artery Embolization in Comparison with Digital Subtraction Angiography. Acad Radiol. 2023 Apr;30(4):689–97.

40. Lucatelli P, Rocco B, Ciaglia S, Teodoli L, Argirò R, Guiu B, Saba L, Vallati G, Spiliopoulos S, Patrone L, Gyánó M, Góg I, Osváth S, Szigeti K, Kiss JP, Catalano C. Possible use of Digital Variance Angiography in Liver Transarterial Chemoembolization: A Retrospective Observational Study. Cardiovasc Intervent Radiol. 2023 May;46(5):635–42.

41. Sótonyi P, Berczeli M, Gyánó M, Legeza P, Mihály Z, Csobay-Novák C, Pataki Á, Juhász V, Góg I, Szigeti K, Osváth S, Kiss JP, Nemes B. Radiation Exposure Reduction by Digital Variance Angiography in Lower Limb Angiography: A Randomized Controlled Trial. J Cardiovasc Dev Dis. 2023 Apr 30;10(5):198.

42. Ansaripour A, Moloney E, Branagan-Harris M, Patrone L, Javanbakht M. Digital variance angiography in patients undergoing lower limb arterial recanalization: cost–effectiveness analysis within the English healthcare setting. J Comp Eff Res. 2024 Apr;13(4):e230068.

43. Góg I, Sótonyi P, Nemes B, Kiss JP, Szigeti K, Osváth S, Gyánó M. Quantitative Comparison of Color-Coded Parametric Imaging Technologies Based on Digital Subtraction and Digital Variance Angiography: A Retrospective Observational Study. J Imaging. 2024 Oct 18;10(10):260.

44. Brenner D, Huda W. Effective dose: a useful concept in diagnostic radiology? Radiat Prot Dosimetry. 2007 Oct 6;128(4):503–8.

45. Martin CJ. Radiation dosimetry for diagnostic medical exposures. Radiat Prot Dosimetry. 2007 Oct 6;128(4):389–412.

46. Andersson M, Eckerman K, Mattsson S. Lifetime attributable risk as an alternative to effective dose to describe the risk of cancer for patients in diagnostic and therapeutic nuclear medicine. Phys Med Biol. 2017 Nov 21;62(24):9177–88.

47. Rand LZ, Kesselheim AS. Controversy Over Using Quality-Adjusted Life-Years In Cost-Effectiveness Analyses: A Systematic Literature Review: Systematic literature review examines the controversy over the use of quality-adjusted life-year in cost-effectiveness analyses. Health Aff (Millwood). 2021 Sept 1;40(9):1402–10.

48. Prieto L, Sacristán JA. Problems and solutions in calculating quality-adjusted life years (QALYs).

49. Paulden M, Sampson C, O'Mahony JF, Spackman E, McCabe C, Round J, Snowsill T. Logical Inconsistencies in the Health Years in Total and Equal Value of Life-Years Gained. Value Health. 2024 Mar;27(3):356–66.

50. Dosimetry in diagnostic radiology: an international code of practice. Vienna: International Atomic Energy Agency; 2007. 359 p. (Technical reports series).

51. Faulkner K, Broadhead DA, Harrison RM. Patient dosimetry measurement methods. Appl Radiat Isot. 1999 Jan;50(1):113–23.

52. Sood A, Forster RA, Archer BJ, Little RC. Neutronics Calculation Advances at Los Alamos: Manhattan Project to Monte Carlo. Nucl Technol. 2021 Dec 3;207(sup1):S100–33.

53. Rogers DWO. Fifty years of Monte Carlo simulations for medical physics. Phys Med Biol. 2006 July 7;51(13):R287–301.

54. Bert J, Sarrut D. Monte Carlo simulations for medical and biomedical applications. In: Biomedical Image Synthesis and Simulation [Internet]. Elsevier; 2022 [cited 2026 Jan 17]. p. 23–53. Available from: https://linkinghub.elsevier.com/retrieve/pii/B9780128243497000104

55. Nocetti D, Villalobos K, Wunderle K. Physical Image Quality Metrics for the Characterization of X-ray Systems Used in Fluoroscopy-Guided Pediatric Cardiac Interventional Procedures: A Systematic Review. Children. 2023 Nov 5;10(11):1784.

56. Doi K. Design Criteria for and Evaluation of Phantoms Employed for Digital Angiography Including Contrast Media Studies. Radiat Prot Dosimetry. 1993 Sept 1;49(1–3):249–55.

57. De Las Heras H, Torres R, Fernández-Soto JM, Vañó E. Objective criteria for acceptability and constancy tests of digital subtraction angiography. Phys Med. 2016 Jan;32(1):272–6.

58. Evaluation and routine testing in medical imaging departments - Part 3-8: Acceptance and constancy tests - Imaging performance of X-ray equipment for radiography and radioscopy. International Electrotechnical Commission; 2024.

59. DIN 6868-4:2021-03, Sicherung der Bildqualität in röntgendiagnostischen Betrieben_- Teil_4: Konstanzprüfung an medizinischen Röntgeneinrichtungen bei Projektionsradiographie mit digitalen Bildempfänger-Systemen und Durchleuchtung [Internet]. DIN Media GmbH; [cited 2025 Dec 5]. Available from: https://www.dinmedia.de/de/-/-/334332686

60. Moores BM, Regulla D. A review of the scientific basis for radiation protection of the patient. Radiat Prot Dosimetry. 2011 Sept 1;147(1–2):22–9.

61. Elek R, Herényi L, Gyánó M, Nemes B, Osváth S. Comparative effectiveness of digital variance and subtraction angiography in lower limb angiography: A Monte Carlo modelling approach. Phys Med. 2024 Dec;128:104859.

62. Alizadeh LS, Vogl TJ, Rafi W, Caruso M, Elek R, Osvath S, Nica A, Gruenewald LD, Yel I, Goekduman A, Koch V, Dimitrova M, D'Angelo T, Booz C. Digital variance angiography enables up to 80% reduction in stationary acquisition radiation dose during prostatic artery embolization: a prospective randomized trial. Eur Radiol [Internet]. 2026 Jan 3 [cited 2026 Jan 9]; Available from: https://link.springer.com/10.1007/s00330-025-12235-3

63. Sótonyi P, Berczeli M, Gyánó M, Legeza P, Mihály Z, Csobay-Novák C, Pataki Á, Juhász V, Góg I, Szigeti K, Osváth S, Kiss JP, Nemes B. Radiation Exposure Reduction by Digital Variance Angiography in Lower Limb Angiography: A Randomized Controlled Trial. J Cardiovasc Dev Dis. 2023 Apr 30;10(5):198.

64. Handbook of Basic Quality Control Tests for Diagnostic Radiology [Internet]. Vienna: International Atomic Energy Agency; 2023 [cited 2024 June 16]. 222 p. (Human Health Series). Available from: https://www.iaea.org/publications/14890/handbook-of-basic-quality-control-tests-for-diagnostic-radiology

65. Anyiszonyan A, Dankó Z, Elek R, Mihályi D, Porubszky T, Váradi C. Útmutató a röntgendiagnosztikai berendezések és képmegjelenítők átvételi és állapotvizsgálatai, valamint állandósági vizsgálatai elvégzéséhez. Nemzeti Népegészségügyi és Gyógyszerészeti Központ; 2022. 214 p.

66. García Balcaza V, Camp A, Badal A, Andersson M, Almen A, Ginjaume M, Duch MA. Fast Monte Carlo codes for occupational dosimetry in interventional radiology. Phys Med. 2021 May;85:166–74.

67. Omar A, Bujila R, Fransson A, Andreo P, Poludniowski G. A framework for organ dose estimation in x-ray angiography and interventional radiology based on dose-related data in DICOM structured reports. Phys Med Biol. 2016 Apr 21;61(8):3063–83.

68. Monte Carlo PENRADIO software for dose calculation in medical imaging. In: 2013 IEEE Nuclear Science Symposium and Medical Imaging Conference (2013 NSS/MIC) [Internet]. Seoul, Korea (South): IEEE; 2013 [cited 2024 Feb 7]. p. 1–7. Available from: http://ieeexplore.ieee.org/document/6829369/

69. Fum WKS, Wong JHD, Tan LK. Monte Carlo-based patient internal dosimetry in fluoroscopy-guided interventional procedures: A review. Phys Med. 2021 Apr;84:228–40.

70. Bujila R, Omar A, Poludniowski G. A validation of SpekPy: A software toolkit for modelling X-ray tube spectra. Phys Med. 2020 July;75:44–54.

71. Poludniowski G, Omar A, Bujila R, Andreo P. Technical Note: SpekPy v2.0—a software toolkit for modeling x-ray tube spectra. Med Phys. 2021 July;48(7):3630–7.

72. Poludniowski G, Landry G, DeBlois F, Evans PM, Verhaegen F. *SpekCalc* : a program to calculate photon spectra from tungsten anode x-ray tubes. Phys Med Biol. 2009 Oct 7;54(19):N433–8.

73. Bissonnette J, Schreiner LJ. A comparison of semiempirical models for generating tungsten target x-ray spectra. Med Phys. 1992 May;19(3):579–82.

74. Hernández G, Fernández F. A model of tungsten anode x-ray spectra: A model of tungsten x-ray anode spectra. Med Phys. 2016 July 19;43(8Part1):4655–64.

75. Boone JM, Seibert JA. An accurate method for computer-generating tungsten anode x-ray spectra from 30 to 140 kV. Med Phys. 1997 Nov;24(11):1661–70.

76. Ay MR, Sarkar S, Shahriari M, Sardari D, Zaidi H. Assessment of different computational models for generation of x-ray spectra in diagnostic radiology and mammography. Med Phys. 2005 June;32(6Part1):1660–75.

77. Bhat M, Pattison J, Bibbo G, Caon M. Diagnostic x-ray spectra: A comparison of spectra generated by different computational methods with a measured spectrum. Med Phys. 1998 Jan;25(1):114–20.

78. Boone JM. Equivalent spectra as a measure of beam quality. Med Phys. 1986 Nov;13(6):861–8.

79. Tucker DM, Barnes GT, Chakraborty DP. Semiempirical model for generating tungsten target x-ray spectra. Med Phys. 1991 Mar;18(2):211–8.

80. Nowotny R, Meghzifene K. Simulation of the effect of anode surface roughness on diagnostic x-ray spectra. Phys Med Biol. 2002 Nov 21;47(22):3973–83.

81. PENELOPE 2018: A code system for Monte Carlo simulation of electron and photon transport: Workshop Proceedings, Barcelona, Spain, 28 January – 1 February 2019 [Internet]. OECD-NEA; 2019 [cited 2023 June 7]. (PENELOPE: A code system for Monte Carlo simulation of electron and photon transport). Available from: https://www.oecd-ilibrary.org/nuclear-energy/penelope-2018-a-code-system-for-monte-carlo-simulation-of-electron-and-photon-transport_32da5043-en

82. Deak PD, Smal Y, Kalender WA. Multisection CT Protocols: Sex- and Age-specific Conversion Factors Used to Determine Effective Dose from Dose-Length Product. Radiology. 2010 Oct;257(1):158–66.

83. Eckerman KF, Ryman JC. External exposure to radionuclides in air, water, and soil. Oak Ridge; 1996. 238 p. (Federal Guidance Report).

84. Tapiovaara M, Siiskonen T. PCXMC: a Monte Carlo program for calculating patient doses in medical x-ray examinations. 2. ed. Helsinki: STUK; 2008. 49 p. (STUK A).

85. DeLorenzo MC, Yang K, Li X, Liu B. Comprehensive evaluation of broad-beam transmission of patient supports from three fluoroscopy-guided interventional systems. Med Phys. 2018 Apr;45(4):1425–32.

86. Malchair F, Dabin J, Deleu M, Merce MS, Bjelac OC, Gallagher A, Maccia C. Review of skin dose calculation software in interventional cardiology. Phys Med. 2020 Dec;80:75–83.

87. Cristy M, Eckerman KF. Specific Absorbed Fractions of Energy at Various Ages From Internal Photon Sources. I. Methods.

88. Cristy M, Eckerman KF. Specific Absorbed Fractions of Energy at Various Ages From Internal Photon Sources. V. Fifteen-Year-Old Male and Adult Female.

89. Cristy M, Eckerman KF. Specific Absorbed Fractions of Energy at Various Ages From Internal Photon Sources. VII. Adult Male.

90. Health Risks from Exposure to Low Levels of Ionizing Radiation: BEIR VII Phase 2 [Internet]. Washington, D.C.: National Academies Press; 2006 [cited 2023 June 7]. 422 p. Available from: http://www.nap.edu/catalog/11340

91. Munoz SR, Bangdiwala SI. Interpretation of Kappa and B statistics measures of agreement. J Appl Stat. 1997 Feb;24(1):105–12.

92. Elek R. Evaluation of a novel imaging method of vessels and moving objects, digital variance angiography. Poster presented at: 5th European Congress of Medical Physics Joint Conference of the DGMP, ÖGMP & SGSMP; 2024.

93. Goode AR, Snyder C, Snyder A, Collins P, DeLorenzo M, Lin P. Signal and contrast to noise ratio evaluation of fluoroscopic loops for interventional fluoroscope quality control. J Appl Clin Med Phys. 2019 Oct;20(10):172–80.

94. Martin CJ, Harrison JD, Rehani MM. Effective dose from radiation exposure in medicine: Past, present, and future. Phys Med. 2020 Nov;79:87–92.

95. Samei E, Järvinen H, Kortesniemi M, Simantirakis G, Goh C, Wallace A, Vano E, Bejan A, Rehani M, Vassileva J. Medical imaging dose optimisation from ground up: expert opinion of an international summit. J Radiol Prot. 2018 Sept;38(3):967–89.

96. McCollough CH, Schueler BA. Calculation of effective dose. Med Phys. 2000 May;27(5):828–37.

97. McCollough CH, Christner JA, Kofler JM. How Effective Is Effective Dose as a Predictor of Radiation Risk? Am J Roentgenol. 2010 Apr;194(4):890–6.

98. Brenner DJ. Effective dose: a flawed concept that could and should be replaced. Br J Radiol. 2008 July;81(967):521–3.

99. Ansaripour A, Moloney E, Branagan-Harris M, Patrone L, Javanbakht M. Digital variance angiography in patients undergoing lower limb arterial recanalization: cost–effectiveness analysis within the English healthcare setting. J Comp Eff Res. 2024 Apr;13(4):e230068.

100. Hendee WR, O'Connor MK. Radiation Risks of Medical Imaging: Separating Fact from Fantasy. Radiology. 2012 Aug;264(2):312–21.

101. Dabin J, Blidéanu V, Ciraj Bjelac O, Deleu M, De Monte F, Feghali JA, Gallagher A, Knežević Ž, Maccia C, Malchair F, Sans Merce M, Simantirakis G. Accuracy of skin dose mapping in interventional cardiology: Comparison of 10 software products following a common protocol. Phys Med. 2021 Feb;82:279–94.

102. Balter S, Hopewell JW, Miller DL, Wagner LK, Zelefsky MJ. Fluoroscopically guided interventional procedures: a review of radiation effects on patients' skin and hair. Radiology. 2010 Feb;254(2):326–41.

103. Bordier C, Klausz R, Desponds L. Patient dose map indications on interventional X-ray systems and validation with Gafchromic XR-RV3 film. Radiat Prot Dosimetry. 2015 Feb 1;163(3):306–18.

104. Kuon E, Glaser C, Dahm JB. Effective techniques for reduction of radiation dosage to patients undergoing invasive cardiac procedures. Br J Radiol. 2003 June;76(906):406–13.

105. Kim HO, Lee BC, Park C, Kim JK, Park WJ, Lee JE, Lim HS, Jeong WG. Occupational dose and associated factors during transarterial chemoembolization of hepatocellular carcinoma using real-time dosimetry: A simple way to reduce radiation exposure. Medicine (Baltimore). 2022 Jan 28;101(4):e28744.

106. Garzón WJ, Andrade G, Dubourcq F, Abud DG, Bredow M, Khoury HJ, Kramer R. Prostatic artery embolization: radiation exposure to patients and staff. J Radiol Prot. 2016 June;36(2):246–54.

107. Ortiz López P, Dauer LT, Loose R, Martin CJ, Miller DL, Vañó E, Doruff M, Padovani R, Massera G, Yoder C. Occupational radiological protection in interventional procedures. London: SAGE; 2018. 118 p. (Annals of the ICRP).

108. Jones AK, Pasciak AS. Calculating the peak skin dose resulting from fluoroscopically guided interventions. Part I: Methods. J Appl Clin Med Phys. 2011 Sept;12(4):231–44.

109. Jones AK, Pasciak AS. Erratum: Calculating the peak skin dose resulting from fluoroscopically guided interventions. Part I: Methods. J Appl Clin Med Phys. 2014 July;15(4):402–402.

110. Ukybassova T, Terzic M, Dotlic J, Imankulova B, Terzic S, Shauyen F, Garzon S, Guo L, Sui L. Evaluation of uterine artery embolization on myoma shrinkage: Results from a large cohort analysis. Gynecol Minim Invasive Ther. 2019;8(4):165.

111. Yo S, Chino M, Hasegawa T, Isshiki T. Actual State of Radiation Exposure During Coronary Angioplasty-A Multicenter Study in the Nationwide Database for Cost Analysis of Percutaneous Transluminal Coronary Angioplasty in Japan-: A Multicenter Study in the Nationwide Database for Cost Analysis of Percutaneous Transluminal Coronary Angioplasty in Japan. Circ J. 2003;67(8):676–81.

112. Noto K, Matsubara K, Koshida K, Iida H, Yamamoto T. Evaluation of patient doses due to fluoroscopic exposures. Radiat Prot Dosimetry. 2011 July 1;146(1–3):234–6.

## 9. Bibliography of the candidate's publications

### 9.1. Publications related to the present work


1. Elek R, Herényi L, Gyánó M, Nemes B, Osváth S. Comparative effectiveness of digital variance and subtraction angiography in lower limb angiography: A Monte Carlo modelling approach. Phys Med. 2024;128:104859. doi:10.1016/j.ejmp.2024.104859

2. Alizadeh LS., Vogl TJ, Rafi W, Caruso M, Elek R, Osvath Sz, Nica A, Gruenewald LD, Yel I, Goekduman A, Koch V, Dimitrova M, D'Angelo T, Booz C. Digital variance angiography enables up to 80% reduction in stationary acquisition radiation dose during prostatic artery embolization: a prospective randomized trial. Eur. Radiol. 2026; doi: 10.1007/s00330-025-12235-3. Epub ahead of print.


### 9.2. Unrelated publications


1. Sudár Á, Pócza T, Elek R, Major T, Tárnoki ÁD, Tárnoki DL, Pesznyák C. Expansion of applicability of multiple scan average dose measurements for CT dosimetry. Phys Med Biol. 2025 Aug 12;70(16). doi: 10.1088/1361-6560/adf40d. PMID: 40706629.

2. Kovács B, Szőnyi-Pákai R, Gáspár L, Elek R. A személyi dozimetria fejlesztése az Izotóp Intézet Kft.-nél, Sugárvédelem, vol. XVII, no. 1, pp. 22–32, 2024.

3. Elek R, Mihályi D, Tóth N, Váradi C, Dankó Z., Balázs E, Sáfrány G, Bágyi P. A nemzeti páciensdózis-felmérő program jelenlegi helyzete, Sugárvédelem, vol. XV., no. 1, pp. 1–11, 2022.

4. Kolozsi Z, Elek R, Pesznyák C. Sugárterhelést befolyásoló tényezők vizsgálata intervenciós radiológiai munkahelyeken, Magyar Radiológia Online, vol. 12, no. 6, pp. 1–12, 2021.

5. Elek R. Egyéni védőeszközök ellenőrzése röntgenmunkahelyeken, Sugárvédelem, vol. XIV. évf. (2021), no. 1. szám, pp. 32–44, 2021.

6. Deme S, Elek R, Pesznyák C, Szűcs L. A pulzált neutronok dózisteljesítményének mérése, Sugárvédelem, vol. XIV. (2021), no. 1, pp. 45–57, 2021.

7. Elek R, Várkonyi I, Kis É, Porubszky T. Újszülöttek és koraszülöttek röntgendiagnosztikai sugárterhelésének vizsgálata mellkasi, hasi és kombinált felvételek során, MAGYAR RADIOLÓGIA, vol. 89, no. 1, pp. 7–15, 2015.

8. Séra T, Porubszky T, Papos M, Elek R, Besenyi Z, Gion K, Bartha A, Pellet S, Pavics L. Validation of CT doses of SPECT/CT and PET/CT hybrid devices: lessons learned, Nuclear Medicine Communications, vol. 35, no. 5, pp. 534–538, 2014.

## 10. Acknowledgements

First of all, I have to express my most sincere gratitude to my supervisor, Szabolcs Osváth, who has taken me to start research on the technology he developed. I cannot express how much knowledge, wisdom and patience did he exhibit throughout my work and how supportive he was. Not only research methods, approaches to scientific work, but the astonishing humane virtue was inspirational he taught me. No matter when and how – even if it was early in the morning, quite late or on the opposite side of the world – he was always available, every time nudging how can he advance the actual issue which I was stuck with. My work could not have been kick-started without his partner, Krisztián Szigeti who once had an ingenuous call to me asking if I can contribute to their investigations into their new imaging technology. I must also mention Levente Herényi who played a key role to support my work and provided valuable discussions. Marcell Gyánó must be mentioned as another key person who assisted me in the experimental work. I wish to thank Miklós Kellermayer for his persistence. The team at Kinepict also deserves accolades for their helpfulness. The image quality test object developed would not exist without the help of István Derka. Without the help of Nándor Fülöp I would not have been able to fix issues in FORTRAN just at the time when hopeless desperation would have taken over.

Finally, I am very grateful for all the women in my family, especially my mother, my wife and my daughter. Their adamantine and most faithful belief trusting me provided the heartland indispensable throughout.